

Topological Quantum Materials for Energy Conversion and Storage

Huixia Luo^{1*}, Peifeng Yu¹, Guowei Li^{2,3*}, Kai Yan^{4*}

¹School of Materials Science and Engineering, State Key Laboratory of Optoelectronic Materials and Technologies, Key Lab of Polymer Composite & Functional Materials, Guangzhou Key Laboratory of Flexible Electronic Materials and Wearable Devices, Sun Yat-Sen University, 135 Xingang Xi Road, Guangzhou 510275, China

²CAS Key Laboratory of Magnetic Materials and Devices, and Zhejiang Province Key Laboratory of Magnetic Materials and Application Technology, Ningbo Institute of Materials Technology and Engineering, Chinese Academy of Sciences, Ningbo 315201, China

³University of Chinese Academy of Sciences, 19 A Yuquan Rd, Shijingshan District, Beijing 100049, China

⁴School of Environmental Science and Engineering, Sun Yat-Sen University, 135 Xingang Xi Road, Guangzhou 510275, China

E-mail: luohx7@mail.sysu.edu.cn; liguowei@nimte.ac.cn; yank9@mail.sysu.edu.cn.

Abstract | Topological quantum materials (TQMs) have symmetry protected band structures with useful electronic properties that have applications in information, sensing, energy, and other technologies. In the past 10 years, applications of TQMs in the field of energy conversion and storage mainly including water splitting, ethanol electro-oxidation, battery, supercapacitor, and relative energy-efficient devices have attracted increasing attention. The novel quantum states in TQMs provide a stable electron bath with high electronic conductivity and carrier mobility, long lifetime, and determined spin states, making TQMs an ideal platform for understanding the surface reactions and looking for highly efficient materials for energy conversion and storage. In this Perspective, we present an overview of the recent progress regarding topological quantum catalysis. We describe the open problems, and the potential applications of TQMs in water splitting, batteries, supercapacitors, and other prospects in energy conversion and storage.

Introduction

Topological quantum materials (TQMs) host symmetrically protected, high mobility electronic states¹⁻⁶. These features make them attractive for a range of applications – most commonly discussed are their potential for spin-related information storage and processing, but TQMs can also be useful for energy conversion and storage. In the past decade, there has been a growing interest in investigating the potential use of TQMs in energy-efficient applications⁷⁻²¹ such as water splitting, thermoelectricity, battery, supercapacitors, and ethanol electro-oxidation. However, the interaction between topological properties and the reaction processes still needs deeper understanding. Further study of topological properties is needed from both a chemistry and physics perspective to uncover the relationship between topological band structures and energy conversion or storage, for the design of high-efficiency heterogeneous catalysts for energy conversion such as water splitting and fuel cells.

In this Perspective, we present a brief overview of the recent development and advances in the use of various TQMs for energy conversion and storage technology. We propose that TQMs could be a new category of energy material for the various utilizations in photo-electrocatalytic water splitting, CO₂ reduction, CO oxidation, battery, supercapacitors, and beyond. We begin by giving a general diagram for catalysis and energy conversion, followed by a review of the recent theoretical research and experimental progress of TQMs for energy conversion and storage. We focus on the applications of TQMs in water splitting, battery and survey the current experimental and theoretical progress. The TQMs used for selective hydrogenation, oxidation of biomass-derived alcohols, storage of hydrogen, and beyond also has been briefly surveyed. In the end, we will give the outlook for the challenge of current topological catalysis and the potential new applications of TQMs. In the Supplementary Information, we provide a brief discussion of the application of TQMs in the thermoelectricity field. For a complimentary review on topological thermoelectric we

direct readers to REF.⁷ and for a review of the topological insulators and thermoelectric, see REF.²² and REF.²³.

Water splitting

Hydrogen is a promising energy carrier due to its large energy density without carbon emission, which is believed as a solution to environmental problems and energy crisis²⁴⁻²⁷. Thus, water electrolysis to produce high-purity hydrogen as the alternative clean fuel to traditional fossil fuels has attracted increased research attention^{28,29}. This process consists of hydrogen evolution reaction (HER) and oxygen evolution reaction (OER), two half-reactions, which can be driven by electricity or light with suitable energy²⁴. HER and OER involve two-electron and four-electron-transfer process which often requires high overpotential (η) to overcome the large energy barrier^{25,26}. Considerable research efforts have been devoted to developing efficient electrocatalysts to improve the electrochemical conversion efficiency and decrease the overpotential of HER as well as OER process. Traditional strategies including defect engineering, nanotechnology, and single atomic technology are proved to be effective in the search for low-cost and high-efficient catalysts³⁰⁻³³. Most key steps in water splitting, such as mass adsorption, electron transfer, and desorption take place on the catalyst surface. Unfortunately, it is still a tough job to tell the origin of catalytic activities and then replace the state-of-the-art noble metal catalysts.

For a typical redox reaction at the crystal surface, electrons are transferred either from the catalysts to the reactant molecules (reduction reaction), or in the reverse direction (oxidation reaction). Thus, the electronic conductivity of catalysts is important because electrons should be passed through the bulk phase and then to the external circuit. In addition, high mobility is necessary to avoid the trapping and recombination of carriers (**BOX 1**). However, the traditional catalysts suffer from surface contamination during the catalytic reaction or poor electronic conductivity, leading to

low catalytic activity or high reaction barriers²⁷. To overcome these problems, the search for novel high-effective catalysts is an urgent need for water splitting.

The topologically protected surface states, giant electron motilities, and chiral surface states of TQMs, make them ideal candidates for catalysis reactions such as water splitting²⁷. The TQMs with robust TSSs can resist perturbations such as defects, a small amount of doping, and surface modifications. Moreover, the TQMs with unique topological electronic band structures can stably supply the topological electrons into the studied catalysts as a robust electron bath. Hence, the TQMs may help to overcome the aforementioned issues for the traditional catalysts. In addition, the out-pointing of p_z components of the p orbital and the d_{z^2} components of the d orbital tend to form covalent bonds with the surface molecules through σ or π bond^{34,35}. Once the electron transfer channel is established, reduction or oxidation reactions can be initiated by applying an electric potential or light illumination. The presence of the surface states has great importance in mediating the interfacial charge transfer and resulting in different reaction pathways depending on the applied potential.

Topological materials for HER

Topological insulators

The research on the catalytic behaviour of TQMs started from the family of 3D topological insulators (TIs) based on bismuth chalcogenides (Bi_2Se_3 and Bi_2Te_3)^{2-4,36}. The response of topological surface states (TSSs) at the surface of Bi_2Se_3 the deposition of metals like Au, Ag, Cu, Pt, and Pd was investigated using DFT calculations³⁷ and improved adsorption energies of oxygen were seen, which indicated the importance of TSSs for the tailored adsorption behaviour. However, this result alone does not suggest optimized catalytic efficiencies because only the metals with original weak reactivity can attain a positive effect from TSSs. This was firstly experimentally and theoretically confirmed by the photocatalytic hydrogen studies on nanostructured Bi_2Se_3 and Bi_2Te_3 catalysts⁸. Benefitting from the high mobility, it was found that the photoexcited

electrons from the TSSs stay for a longer time than their counterpart compounds (such as Bi_2Se_3 , Bi_2Te_3 , $\text{Bi}_2\text{Te}_2\text{Se}$), which leads to efficient electron-hole separation, then giving rise to the high-effective photochemical HER performance⁸. The effect of TSSs can be maximized by making highly-crystalline thin films with desired exposing crystal surfaces. For example, Bi_2Te_3 and SnTe thin films exhibited remarkable intrinsic HER activities and maintained high stability against slight surface oxidation and defects^{38,39}. More interesting, the TSSs could not only interact with the adsorbed hydrogen directly, but they can also change the catalytic performance of the deposited catalysts⁴⁰. The Pd (20 nm)/SnTe (70 nm) heterostructure fabricated by molecular beam epitaxy displays much better HER performance and turnover frequency of per-Pd-site in comparison with the Pd (20 nm) thin film and is even superior to the commercial Pt foil. Such a good HER activity is the result of the transfer of electrons from both the Pd surface and the adsorbed H atoms to the TSSs adhered to the SnTe (001) underlayer, which leads to the weaker Pd-H binding strength and more favourable hydrogen adsorption free energies⁴¹. These findings also indicate that it is not technically a requirement for the direct bonding between the TSSs and adsorbates.

Topological semimetals

A hindrance to the application of TIs as catalysts is the low chemical stability of metal chalcogenides. Although the topological surface properties are protected by their symmetry, they can be destroyed under harsh catalytic conditions. The upmost few layers of air-exposed Bi_2Se_3 TIs at ambient temperature could be reconstructed and can be even completely vanished in the acidic/alkaline electrolytes. This will significantly decrease the contribution of TSSs in the catalysis reactions^{42,43}. In addition, the bulk phase of TIs is characterized by a bandgap like the conventional semiconductors, albeit the bandgaps are generally not big, and the crystal surfaces are metallic⁴⁴. The low conductivity of the bulk phase will increase the charge transfer resistance or lower the charge-hole separation efficiencies when used as catalysis, and thus are detrimental to the catalytic kinetics. With this in mind, topological semimetals received increasing

research interest because of their high chemical stability and relatively high electronic conductivity. Topological semimetals (TSMs), mainly including Weyl semimetals (WSMs), Dirac semimetals (DSMs) and nodal line semimetals (NLSMs) appear at the borderline between topological and trivial insulators and have become the major members of TQMs^{45,46}. It has been noticed that the existence of conducting TSSs cannot assure good catalytic performances. The weak interaction between TSSs and adsorbates will lead to low coverages and slow catalytic reaction kinetics^{38,47,48}. Potential TQMs catalysts need to be able to boycott turbulence under surface modification while having high electronic conductivity and carrier mobilities for the fast electron transport during the catalytic reaction process. The robust TSSs of TSMs with high electronic conductivity and carrier mobilities may promote the catalytic activity.

Application of the TSMs with high carrier mobilities for water splitting was firstly realized in the photocatalyst materials, transition-metal monophosphides WSMs (TaP, NbP, TaAs and NbAs)⁴⁹. The carrier mobility of these transition-metal monophosphides is in the order of $10^5 \text{ cm}^2 \text{ V}^{-1} \text{ s}^{-1}$ (Table 1). Such high mobility boosts fast transfer between TSSs and surface adsorbates, leading to high catalytic activity⁵⁰. Subsequently, Pt-containing TSMs (PtSn₄, PtAl, and PtGa) with high carrier mobilities were also documented to show superior HER catalytic performance, even exceeding those of some noble metal-containing catalysts^{13,16}. In addition, group VIII noble-metal dichalcogenides (PtSe₂, PdTe₂, and PtTe₂) have recently been theoretically predicted and experimentally confirmed to be DSMs and host type-II Dirac fermions⁵¹⁻⁵⁴.

It also has been theoretically proposed that the double vacancies in Se or Te (DV_{Se} or DV_{Te}) of DSMs and boron-substitution can adjust the interplay between H and basal plane and then boost the HER performance of these monolayer noble-metal dichalcogenides⁵⁵. In particular, the Gibbs free energy for hydrogen adsorption is decreased from 0.94 eV for the pristine PdSe₂, to only 0.02 eV with 2 % boron substitution. This corresponds to fourteen orders of magnitude increase in the exchange current density after doping. In addition, it is well-known that the topological band structures are robust against surface modification such as elemental doping, defects, surface atomic reconstruction, surface oxidation, and molecules adsorption. For

example, adding Na vacancies to the DSM Na_3Bi Shifted the Fermi level upward, but the bulk Dirac cone persisted despite heavy surface modification⁵⁶. Similarly, the TSSs of the TI Bi_2Se_3 is stable against N_2 and air exposure, and even oxidation⁵⁷. Therefore, the interaction between the variations of TSSs and the enhanced HER catalytic activities of these noble-metal dichalcogenides is worth further study.

It should be noted that the traditional Pd-based electrode is not an ideal electrocatalyst for HER due to the formation of metal hydride^{58,59}. The presence of the robust TSSs seems to not only reduce the metal hydride effect but also enhance the HER catalytic activities and stabilities, as seen in the case of the topological and superconducting α -BiPd catalyst, which shows a striking improvement of the catalytic activity and stability. It is found that α -BiPd shows a shorter Pd-Pd bond in comparison with the pure Pd metal, which leads to the large density of states with conduction electron at the Fermi level^{60,61}.

The cost and abundance of the catalysts in practical usages should be also taken into consideration besides the catalytic activity, selectivity, and stability. Recently, the noble metals-free TSMs have also been found to show excellent HER catalyst candidates⁶²⁻⁶⁴. Especially, the low-dimensional transition metal dichalcogenide (TMD) system is one of the most extensively studied topological semimetals due to its low dimensional structure and rich topological properties. For example, the bulk orthorhombic T_d - MoTe_2 TMD is type-II WSM⁶⁵⁻⁶⁹, while the monolayer and few-layers two-dimensional (2D) $1T'$ - MX_2 ($M = \text{W}, \text{Mo}$; $X = \text{Te}, \text{Se}, \text{or S}$) have nontrivial Z_2 topological invariants with quantum spin Hall (QSH) effect feature^{70,71}, although bulk $1T'$ - MoS_2 is semiconducting with a fundamental gap ($E_g \approx 0.08$ eV). Early photocatalytic measurements of the topological 2D $1T'$ - MoTe_2 TMD provide support for the topological heterogeneous catalysis in water splitting⁶². Later work finds that topological 2D $1T'$ - MoTe_2 nanosheets were also good for electrocatalytic hydrogen generation, where both the single-crystal and polycrystalline 2D $1T'$ - MoTe_2 nanosheets display remarkable performance for hydrogen evolution⁶⁴.

Size reduction can enhance the catalytic properties of TQMs, for example, an improvement in the HER activity has been observed in the polycrystalline powder materials with smaller sizes compared to the single crystals with larger sizes^{62,64}. Hence, it can be expected that the catalytic performance of WSMs can further be promoted largely by decreasing the particle size, for instance, by constructing them as nanoparticles until the bulk remains metallic. Recently, noble metals-free VAl_3 -based topological semimetals with large carrier mobility at room temperature were also verified to be highly-effective and acid-stable topological catalysts, where the direct transfer of electrons from the occupied robust TSSs to the adsorbed H boost the electrochemical HER efficiency⁶³. These results affirm that the enhancement of the HER activity in these noble metals-free TQMs is a result of the TSSs and the high mobility.

d-band topological materials

Although great progress has been made in previous works on employing TQMs in HER, most of these TSSs are derived from the sp band of topologically trivial metal catalysts rather than the d band. However, based on the traditional adsorption mechanism, the d band figures prominently in determining catalytic efficiency⁷². This is because only the d orbitals could form strong bonding with the surface adsorbates. Otherwise, the adsorption is not energetically favored and leads to low reactant coverage, which will decrease the intrinsic activities of the catalysts.

Therefore, TQMs in which the TSSs are derived from the d band may be beneficial to the catalytic activity. The observation of unconventional topological fermions (such as chiral fermions, topological non-Fermi liquid, Dirac nodal line, large topological Fermi arcs, and so on) in the group of transition-metal monosilicides has received increasing research attention⁷³⁻⁷⁸. It is interesting to see that the TSSs are mainly derived from the transition metal d orbitals. More importantly, they are also accompanied by large topological non-trivial energy windows and a large density of states around the Fermi level^{79,80}. This suggests an enlarged contribution of TSSs in the catalysis

reactions. One example of a transition-metal monosilicide is CoSi., which belongs to the space group of $P2_13$ with a cubic structure, where each Co atom is connected with six Si atoms and vice versa (**Fig. 1a**). Based on the first principle calculations prediction, and supported with later ARPES experimental evidence, it is found that peculiar massless fermionic excitations with nonzero Berry flux such as spin-1 excitations with threefold degeneracy and spin $-3/2$ Rarita-Schwinger-Weyl fermions coexist in the transition metal silicide CoSi (**Fig. 1b**) (REFS^{75,77}).

Recently, a group of transition-metal monosilicides (MSi , $M = \text{Co, Ni, Ti, Fe, Mn, Rh, and Ru}$) has been synthesized by the arc-melting method within several minutes and the easily fabricated MSi polycrystalline electrodes display remarkable activities in the HER process with overpotentials of $34 \sim 54$ mV at the current density of 10 mA cm^{-2} as well as low Tafel slopes of $23.6 \sim 32.3 \text{ mV dec}^{-1}$ (see REF.¹¹). These are similar or even superior to $37 \text{ mV, } 26.1 \text{ mV dec}^{-1}$ of 20 wt% Pt/C (**Fig. 1c**). The theory calculations confirm the outstanding activities are closely related to hydrogen coverages ($\sim 100 \%$) on several low surface energy facets. When compare the free energy difference $|\Delta G|$ of the previously reported topological catalyst with the commercial Pt in a volcano plot, the free energy difference $|\Delta G|$ of transition-metal monosilicides is close to the commercial Pt catalyst sitting near the peak of the volcano plot (**Fig. 1d**). The subtle deviation of the hydrogen adsorption energy and the free energy difference $|\Delta G|$ of these MSi are mainly contributing to the transition metals filled by the different d orbital.

Furthermore, catalytic properties can be tuned and enhanced by various alloying combinations, which opens a new avenue to use low-cost silicon-based candidates for HER. This is maybe a good sample for the explanation of the enhancement of the HER activity by the combination of the nontrivial TSSs and the conditional d band theory (see REF.¹¹). However, the link between robust TSSs and the high HER catalytic activity still needs to be fully understood. Recently, it is found that topological charge carriers in NiSi WSMs with hybrid Weyl states and long surface Fermi arcs close to the Fermi level indeed take part in the HER process (**Fig. 1e**). In the comparison of the surface band structure of NiSi without and with H adsorption, four Weyl node points

shift down on the NiSi surface with H atoms and the Fermi arcs shifts toward lower energy after H adsorption, indicating that the charge transfer takes place on its surface and the charge exchange between NiSi surface and H atom in the HER process (**Fig. 1f**)⁸¹. These results further indicate that it is highly possible to design HER catalysts without noble metals via topological engineering of the band structure.

Topological materials for OER

Compared to the topological HER catalysts, topological OER catalysts have been less studied so far, although numerous excellent OER catalysts have been discovered by introducing applying strain, vacancies, defects, doping, or tuning transition-metal coordination. However, as these strategies rely on extrinsic disturbances, they are closely paired with structural instability, leading to the instability of the OER activities. In the OER process, the adsorption of diverse reaction intermediates and electronic structures has an important effect on regulating the adsorption processes. Based on the Shao-Horn (SH) principle, the orbital filling, e_g affects the binding energy of oxygen intermediates to the catalyst surface and changes the OER performance; hence we can tune the e_g of metal sites to optimize OER activities⁸² (**Fig. 2a**). Recently, ternary Heusler compounds have been successfully documented to be excellent OER catalysts by precisely controlling e_g (**Fig. 2b**) (REF.⁸³). Another prominent example is the TSM $\text{Co}_3\text{Sn}_2\text{S}_2$ bulk single crystals with high electrical conductivity and robust surface states at room temperature. The TSSs are mainly derived from the Co $3d$ orbitals in the Kagome lattices and are just located above the Fermi level (**Fig. 2c**). The bulk single crystals with TSSs display eminent OER catalytic activity and even surpass the Co-based nanostructured catalysts, although the specific surface area of the bulk single crystal is much smaller. The high efficiency of the bulk single crystals can be explained by the half-filled Co e_g orbital in the TSSs, which are pointing towards the p orbital of the adsorbed hydroxide ions. Such an $e_g - p$ orbital overlap will strengthen the bonding between the active sites and the adsorbates and make the electron transfer more efficiently through the bonds, thereby resulting in the high OER performance of the

$\text{Co}_3\text{Sn}_2\text{S}_2$ bulk single crystals and comparable to the state-of-art RuO_2 catalysts (**Fig. 2d**) (REF.¹²). These findings highlighted the significance of using TSSs as the catalytic active sites in the design of high-efficient catalysts.

Batteries and supercapacitors

Lithium-ion batteries

TQMs with symmetry-enforced Dirac states provide robust carriers for high electronic conductivity and can improve battery efficiency. Many topological carbon-rich compounds are theoretically predicted to be good anodes for lithium-ion batteries (LIBs) when compared with conventional carbon compounds such as graphite, carbon nanotubes or porous carbon nanofibers (See Table 2). In fact, these carbon compounds have been extensively used as anodes for LIBs owing to their excellent reversibility, low environmental impact, and cost⁸⁴. In particular, porous carbon compounds are useful because of their big specific surface area, which can offer abundant binding sites for Li-ions and thus favours high-capacity LIB anodes. The traditional porous carbon candidates used in LIBs are commonly amorphous⁸⁵, where the disordered holes and defects have an impact on the diffusion of Li-ions and the irreversible capacity is usually high⁸⁶.

There are numerous theoretical discussions on the use of topological semi-metallic porous carbon materials as potential LIBs anodes, but the influence of TSSs needs to be further studied experimentally⁸⁷⁻⁹¹. It has been found that these all-carbon-based porous 3D topological carbon compounds with inherently ordered porosity possess higher electrical conductivity^{92,93} in comparison with the conventional disordered porous carbon compounds and hence are beneficial for anode components. The use of the topological semi-metallic porous carbon materials for LIBs has its roots in the pioneering work in REF. 87. From this work, the all-carbon-based porous body-centered orthorhombic C_{16} (bco- C_{16}) as a high-effective LIB anode candidate could be

understood as a consequence of a novel topological NLSM bco-C₁₆ (**Fig. 3a, b**) with intrinsic high electronic conductivity⁸⁹ and 1D migration channels (**Fig. 3c**). The ion diffusion channels in bco-C₁₆ are immune to the compressive and tensile strains during charging/discharging, which leads to a larger specific capacity (the maximum Li concentration, Li-C₄) than that of the usually employed graphite anode (Li-C₆). Furthermore, the energy barrier declines with enhancing Li insertion and can achieve 0.019 eV at large Li-ion content; the average voltage is very low (0.23 V), and the volume change during the test keeps pace with that of graphite⁸⁷ (**Fig. 3d**). bco-C₁₆ has a larger volume expansion (13.4 %) than that of the usually utilized graphite anode (10 %).

Later work⁹⁴ proposes a porous 3D nodal line semimetal carbon (termed HZGM-42) as a potential anode compound for LIBs, which shows a large theoretical specific capacity (637.71 mAh g⁻¹) and a small energy barrier (0.02 eV) for Li-ion transport along the ordered 1D channels as well as a subtle volume change (2.4%) during charging and discharging processes. This performance is the result of the larger pore size in topological porous carbon HZGM-42 with hexagonal symmetry compared to the interlayer distance in graphite and intrinsic superior electrical conductivity in comparison with the disordered carbon, metal oxide, metal sulfide, and selenide anodes⁹⁵⁻⁹⁷.

One year after the discovery of porous nodal line semimetallic carbon, monoclinic C₁₆ (m-C₁₆)⁹⁸, it is noticed that m-C₁₆ exhibited superior performance as an anode compound for LIBs to that of the previously reported bco-C₁₆. TQM m-C₁₆ possesses a similar specific capacity (558 mAh g⁻¹) but with a smaller volume change (3.6%) during the charging/discharging performance and a lower Li-ion transport energy barrier (0.25 eV) when compared to corresponding values of 558 mAh g⁻¹, 0.53 eV and 13.4% in bco-C₁₆ (REF.⁸⁸). The Li atoms contribute nearly all valence electrons to TQM m-C₁₆, resulting in a strong ionic bonding with the substrate and consequent ascendant performance.

With the prediction of the topological porous carbon as LIB anode materials, it is natural to ask whether they can be realized experimentally. There has been a proposal

to use a high-pressure synthesis technique with the universal structure database to seek a topological semimetal porous carbon as the expected anode. It is found that an orthorhombic phase LiC_6 with uniform pores can be acquired at 30 GPa. In addition, the obtained carbon structure after removing the Li atoms is still a topological semimetal with an interlocked graphene network (IGN) and an inherent large electronic conductivity. A low Li-ion diffusion energy barrier and three orders of magnitude higher diffusion coefficient ($10^{-4} \text{ cm}^2 \text{ s}^{-1}$) than that of graphite anode are observed at both small and large Li concentrations in the IGN. Besides, the volume changes during the Li insertion/extraction processes are as low as 3.2% and keep the same theoretical specific capacity as that of graphite anode⁹⁹.

Sodium-ion batteries

An alternative to LIBs is sodium-ion batteries (NIBs), as sodium is abundant and inexpensive compared to lithium. Similar to the aforementioned LIBs cases, the 3D porous topological carbon material, tetragonal C_{24} (tC_{24}) with two topological nodal surfaces crossing the whole Brillouin zone, recently have been predicted to be a potential anode compound for NIBs. tC_{24} has a long cycling life, a high predicted capacity of $232.65 \text{ mAh g}^{-1}$, an appropriate average voltage of 0.54 eV, a low diffusion energy barrier for Na ions and a negligible volume change ($\sim 0.94\%$) during the charge/discharge processes⁹⁰. There are three distinct voltage regions for varying Na content in $\text{Na}_x\text{tC}_{24}$ and the voltage maintains positive during the whole operation, indicating that the half-cell reaction can occur automatically to achieve the ultimate component (Na_5C_{48}) (**Fig 3e**). Therefore, the tC_{24} anode can have a wholly reversible capacity of $232.65 \text{ mAh g}^{-1}$ (REF.⁹⁰). The aforementioned 3D NLS porous carbon HZGM-42 is a potential anode candidate not only for LIBs but also for NIBs with high performance¹⁰⁰. All these facts indicate that the all-carbon HZGM-42 with large energy density, excellent rate capability as well as good cycling stability can be used as a versatile anode candidate for both LIBs and NIBs.

In contrast to porous topological carbon materials, the topological silicon materials employed as anode materials for NIBs have attracted less attention, despite silicon and carbon being located in the same group in the periodic table. Recently, it has been found that the all-silicon NLSM consisting of interpenetrating silicene networks, is a potential material for NIBs anode due to its comparatively big storage voltage (1.35 V), inherent metallic property together with particularly small barrier energy (5.2 meV), and subtle volume change¹⁰¹. More impressively, hexagonal supertetrahedral-boron consisting of B₄ cluster is first proposed to be a 3D porous topological metal with several kinds of spin-orbit-free burgeoning fermions (REF.¹⁰²) and subsequently is found to be an anode compound for both LIBs and NIBs with an ultrahigh capacity of 930 mAh g⁻¹, low migration barrier of 0.15 and 0.22 eV and low volume changes of 0.6 % and 9.8 % for Li and Na ions, respectively¹⁰³. These enchanting characteristics imply that 3D porous TQMs deserve further investigation for battery devices¹⁰⁴.

Recently, Bi₂Te₃ is utilized for sodium storage (**Fig. 3f**). Based on the *in-situ* XRD characterization, there exists a four-step crystallographic phase-change mechanism of Bi₂Te₃ during sodiation/dissociation processes. After that, the WSM T_d-Wte₂ was applied as the electrode material for NIBs, which delivers a 245 mAh g⁻¹ at 100 mA g⁻¹ (REF.¹⁰⁵). The Na-based TQMs also provide new promising material candidates for NIBs. For instance, NaAlSi and NaAlGe which are dual double NLSs (those that have both type-I nodal lines and type-III nodal points) are theoretically predicted to be potential candidates for NIBs, due to their large proportion of Na ion, with a predicted reversible capacity of 476 and 238 mAh g⁻¹, respectively (see **Fig. 3e** in REF.⁹¹).

Furthermore, 3D DSMs, such as Na₃Bi, host 3D Dirac fermions that are immune to in situ surface K-doping⁵⁵. Thus 3D DSMs have a theoretical capacity of 385 mAh g⁻¹ (REFS^{106,107}). Besides, a topological phase transition from DSMs to a trivial band insulating compound by alloying has been observed in Na₃Bi_xSb_{1-x} alloys, which is derived from the strength of the spin-orbit-coupling (SOC) by varying with Sb content. The topological state-driven from SOC in Na₃Bi is very robust compared to anode material Na₃Sb. The presence of Dirac bands with high carrier velocities and the associated conductivity offer a favorable factor for battery performance¹⁰⁸.

There is a large number of existing materials are theoretically predicted or experimentally confirmed to be TQMs^{4,6,36,109,110,111}. But, what kinds of TQMs are promising to be candidate battery materials? This question has been approached using machine learning theory to go through 7300 TQMs for promising NIBs cathodes, and then using DFT calculations to confirm them¹¹⁰. If a TQM cathode ensures large electrical conductivity, then large ionic conductivity is required for high-efficient activity. Building on this idea, in Ref 110, a descriptor-based machine learning model involving atomic radius, Pauling electronegativity, many valence electrons, first ionic energy, and radial basis functions and a supervised Gaussian Process Regression (GPR) model, is used to predict the Na-ion migration energy barrier for the topological NIB candidates. The data mining displays that the atomic radius plays an important role in the migration energy barrier, and the cations affect more significantly than anions for Na ion migration. This calculation provides a powerful and simple rule for further search for new topological battery cathode materials¹¹⁰.

Potassium-ion batteries

Potassium-ion batteries (KIBs) have also been considered as one of the possible substitutions for LIB due to the negative potential of the K^+/K redox couple, the considerably adequate resources of K, and the practicable usage of low-cost aluminum (Al) current collector in KIBs. The discovery of inherent porosity-ordered channels and large electronic conductivity in the topological carbon compounds led to the proposal of a 3D porous NLSs carbon allotrope (named BDL-14) as a promising KIB anode. The topological BDL-14 shows superior properties of anodes to those of the anodes currently being considered¹¹².

Aqueous zinc-ion batteries

Aqueous ZIBs (AZIBs) are also considered to be a promising alternative to the widely used LIBs in large-scale electrical energy storage systems because of the cheap, high safety, and atoxic nature of zinc. One significant factor that demands further development is finding electrode materials that store Zn^{2+} ions with large invertibility and rapid kinetics¹¹³. WSMs with excellent electrical conductivity and high carrier density around the Fermi level are appealing candidates for AZIBs, benefiting from TSSs. The Weyl semimetal, $\text{Co}_3\text{Sn}_2\text{S}_2$, is recently proposed to be an AZIB cathode with a discharge plateau near 1.5 V. Furthermore, more Zn^{2+} transfer channels and enhancing charge-storage kinetics as well as higher Zn^{2+} storage ability are obtained by the introduction of Sn vacancies. The synergy benefits of leveraging TSSs and introducing vacancies have been realized in the $\text{Co}_3\text{Sn}_2\text{S}_2$ battery performance¹¹⁴.

Supercapacitors

Apart from ion batteries, TQMs also offer new opportunities in other high-efficient energy storage devices such as spin battery¹⁷ and supercapacitors¹¹⁵. In the last 5 years, supercapacitors have gained incalculable attention owing to their large power density, rapid charge/discharge rates, and excellent cycling stability, all features show great potential for bridging supercapacitors and batteries. According to the different storage mechanisms, supercapacitors can be decided into two classifications: electrochemical double-layer capacitors involving reversible ion adsorption/desorption on the electrode-electrolyte interface and pseudo-capacitors, which depend upon the Faradaic redox reactions. Currently, layered 2D Bi_2Se_3 nanosheets are used for supercapacitors and exhibit a specific capacitance of 439 F g^{-1} at 4 A g^{-1} (REF.¹¹⁶). When $\text{MoSe}_2/\text{Bi}_2\text{Se}_3$ hybrid nanosheets are used for supercapacitors, they give capacitance of 1451.8 F g^{-1} at 1 A g^{-1} and maintain 750 F g^{-1} at 20 A g^{-1} (REF.¹¹⁷). Another example is the TMD tungsten ditelluride ($1\text{T}_d\text{-WTe}_2$), which has been first

theoretically predicted¹¹⁸ and subsequently experimentally documented to be a type-II Weyl semimetal¹¹⁹⁻¹²¹, showing a promising advanced electrode used in all-solid-state pliable supercapacitors. In this case, 1T_d-WTe₂ single-crystal bulk is exfoliated into nanosheets by liquid-phase exfoliation and then fabricated into air-stable films by drop-casting 1T_d WTe₂ nanosheets on various substrates including Au/Ti coated PET substrate and Si/SiO₂ wafer, which acts as the electrode directly. The films are then assembled into all-solid-state pliable supercapacitors by using a gel electrolyte of poly(vinylalcohol)/H₃PO₄ (PVA/H₃PO₄) sandwiched between two films, which show superior performance to the commercial 4V/500 μAh thin-film LIB and 3V/300 μAh Al capacitor, accompanied by splendid flexibility and excellent cyclability¹¹⁵. These facts further verify that the TQMs offer new material platforms to explore the battery devices.

Multi-electron transfer reactions

Catalysis for CO₂ conversion

TQMs with TSSs are not only good candidates for single electron transfer reactions such as HER but also proved to be efficient in multi-electron processes including carbon monoxide (CO) oxidation¹²², carbon dioxide (CO₂) electro-reduction^{123,124}, and selective hydrogenation of alkynes^{125,126}. An early study employs gold-covered 3D Bi₂Se₃ as a prototype example for CO oxidation¹²². Based on first-principles DFT calculations, it is found that the TSSs serves as a highly-effective electron bath. The dissociation and adsorption of O₂ and CO molecules on a gold-covered Bi₂Se₃ structure can be promoted by raising the adsorption energies of these molecules. Later, the experimental study of the influence of TSSs on various surface reactivity in Pd-covered Bi₂Te₃ is reported which agreed well with the aforementioned theoretical predictions¹²⁷. Moreover, the theoretical results imply that the TSSs from Bi₂Te₃ can tunnel through a thin Pd layer and remarkably boost the surface activity of

Pd¹²⁷. Bismuth, which is a topological crystalline insulator, can be dissolved under HER conditions and is not suitable for water electrocatalysis. But the Bi nanostructures with exposed surface states are one of the most efficient catalysts for CO₂ reduction which exhibited a small overpotential and high selectivity of Faradic efficiency over 92.2% in a wide partial current density range from 9.8 to 290.1 mA cm⁻² (REF.¹²⁸). The topological surface states preferentially adsorbed *OCHO and mitigate the competing adsorption of *H in the reaction process.

The family of noble metal dioxides (such as RuO₂ and IrO₂) is a well-known catalyst and has been employed in a widely heterogeneous catalytic reaction including the oxidation of CO and NO_x, the gradation of alcohols, and dehydrogenates NH₃, anodic evolution of chlorine in Deacon process and so on¹²⁹⁻¹³³. More interestingly, the IrO₂ and RuO₂ binary oxides recently have been confirmed to have Dirac nodal lines and exhibit a large spin Hall effect or a crystal Hall effect¹³⁴⁻¹³⁶. The surface adsorption activities of H₂, O₂, NO, and CO in the active (110) surface of RuO₂ have been studied by in operando APRES. It is found that RuO₂ (110) can oxidize CO and H₂, but can't afford to oxidize NO, implying the active role of the flat-band surface states in catalytic charge transfer processes at the oxygen bridge sites¹³⁷. This approach further provides helps to search for more effective topological catalysts. However, this method still has limitations. Whether topology and/or correlation physics such as magnetism impact surface activities of TQMs, is still hard to be detected by ARPES experimentally so far. Distinguished from the DSMs (like Na₃Bi and Cd₃As₂), the cubic antiperovskite material Cu₃PdN has been recently predicted to be a 3D nodal line semimetal¹³⁸ and a possible topological superconductor¹³⁹. Cu₃PdN with rich physical properties also has a superior electrocatalytic activity for CO₂ reduction to formic acid to the non-topological compounds Cu₃N and Cu₃Pd (REF.¹⁴⁰). In addition, Cu₃PdN is a potential candidate for oxygen reduction reaction (ORR) under alkaline conditions¹⁴¹. The effect of TSSs in Cu₃PdN on these heterogeneous catalytic reactions has not been considered and uncovered for this moment. Recently, 2D topological metal monolayer β -PdBi₂ is also reported to show outstanding catalytic performance for CO₂ electro-reduction to formic acid, where the additional electronic states at the Fermi level caused by the

inherent SOC effect remarkably improve the adsorption of OCHO* intermediate on β -PdBi₂ monolayer, resulting in the low potential of -0.26 V vs. reversible hydrogen electrode (RHE) for CO₂ electro-reduction to formic acid (REF.¹²⁴). APRES has been recently used to characterize the Dirac nodal-line fermions in the Cu₂Si monolayer (REFS^{142,143}). Accordingly, 2D topological Cu₂Si nanoribbons with a chair form edge (marked as A > CuSi) and a serrated edge winding-up of Cu or Si (marked as Z > Cu and Z > Si) can reduce carbon dioxide to *COOH with small barriers due to the edge-state-enhanced conductivity in NLSMs. Specifically, S > Si is most active for further hydrogenation, exhibiting the capability of transporting eight electrons to yield methane with a small free energy variation of 0.24 eV (Fig. 4a). For CO₂ conversion reactions, the side reaction of HER should be taken into consideration as it is generally more thermodynamically favorable. It is interesting to see that DNLs Cu₂Si exhibited high selectivity towards the target reaction of CO₂ reduction. As displayed in Fig. 4b, the free energy change of HER is 0.36 eV at the Z > Si site, which is significantly larger than the target reaction with the value of 0.24 eV(REF.¹⁴⁴). This suggests that the CO₂ reaction is more thermodynamically favorable and the side reaction can be inhibited efficiently.

Organic molecules conversions

The superconductor and type-II Dirac semimetal, PdTe₂ has been used for ethanol electrooxidation (EOR) and the mass activity of PdTe₂ nanosheet electrocatalyst is increased by about quintupling as compared with that of commercial Pd black (**Fig. 4c**). Moreover, the forward current (J_f) and backward current (J_b) of PdTe₂ electrocatalyst in the proportion of 5.28:1, which is much larger than previously observed ($J_f/J_b \approx 2$), suggesting outstanding oxidation completeness of ethanol. Besides, PdTe₂ topological electrocatalyst exhibits a low Tafel slope (41.2 mV dec⁻¹) and comparable durability (see **Fig. 4d**)¹⁰.

Selective hydrogenation is a significant reaction in the pharmaceutical and petrochemical fields. It is of particular importance in the polyethylene production

processes, where the removal of alkyne impurities from alkene feedstock is vital to inhibit the poisoning of the heterogeneous catalyst during alkene polymerization. Recently, some TQMs (such as PtGa chiral crystal, $\text{Co}_2\text{Mn}_x\text{Fe}_{1-x}\text{Ge}$ Heusler alloys) also have been considered as new catalysts for the selective hydrogenation of alkynes based on the conventional *d* band theory with the Brønsted-Evans-Polanyi (BEP) relation^{125,145}. Yet, there is a lack of discussions on the relationship between TSSs and catalytic performance.

As shown in the aforementioned section on water splitting, the TQMs with robust TSSs and high mobility are in favour of the HER and OER processes. In addition, recently, it has been found that the TQMs with robust conductivity protected by topology also can keep in the storage of hydrogen. The excellent hydrogen storage performance in Li_2CrN_2 (REF.¹⁴⁶) (**Fig. 4e**) sheet with a gravimetric capacity of 4.77% is observed (**Fig. 4f**), which is superior to the Li decorated MoS_2 (4.4%) and Li-decorated phosphorene (4.4%). Besides, the hydrogen adsorption energy within the area of 0.16 - 0.33 eV is in the requisite energy area for the balance of the adsorption stability and fast kinetics, meanwhile, the releasing temperature within the area of 160 - 270 K is preferable for practical usages¹⁴⁷.

TQMs have been rationally designed as robust catalysts for the selective hydrogenation and oxidation of biomass-derived alcohols (like furfuryl alcohol and benzyl alcohol), acid (such as levulinic acid), and aldehydes (for example, furfural, cinnamaldehyde, and benzaldehyde). Fine Pd, Pt, Cu nanoparticles (less than 10 nm) mainly exhibited (111) crystal plane have exhibited good performance in the hydrogenation of biomass-derived levulinic acid and furfural, whereas biofuel component gamma-valerlactone (over 98% yield) and 2-methyl furan (over 55%) were selectively produced. This superior performance is closely related to the tempting electronic properties of TQMs as well as the unsaturated *d*-band in enhancing the adsorption of reactants and hydrogen¹⁴⁸⁻¹⁵⁰.

Outlook

Topological quantum catalysts use the topologically protected surface bands as active sites, which is different from the edge-, vacancy-, dopant-, strain-, or heterostructure-created sites. This will allow us to understand and identify the origin of catalytic activities. The topological properties of TQMs also meet the criteria of high-performance battery materials, supercapacitors, and thermoelectrics, and thus they have been received increasing research efforts. Thanks to the rapid progress in topological theories such as topological quantum chemistry, the high-throughput first-principles calculations are powerful in searching and identifying topological materials, with several databases have been established^{4,151,152}. Researchers can identify the topological properties and band structures fast and precisely from the databases now, although improvements are still needed.

Even though the research on TQMs for energy conversion and storage is developing rapidly, this field is still immature, especially in terms of their relationships between topological states and energy conversion as well as storage processes derived from topological states. Unlike the exploration of topological properties such as resistivities and various Hall effects, the chemical reactions are generally happening in critical conditions such as acidic, alkaline, and even high vacuum. This makes the in-situ observation of topological effects an extremely difficult task now. To find direct evidence, high-quality bulk single crystals and in-situ monitoring of the band topology evolution using spectroscopy are urgently needed. A good example is the study on the extensively investigated MoTe₂. With non-topological 2H-MoTe₂ and topological 1T'-MoTe₂, it is possible to isolate the contribution from the topological phase by tracking the change of surface compositions, conductivities, carrier mobilities, and Hall resistivities before and after electro/photocatalytic reactions¹⁵³. In addition, in-situ tools (such as EXAFS, TEM, nano-ARPES) combined with theoretical calculations are highly desirable. It has been preliminary confirmed that ARPES is powerful to track the response of bulk DSMs and TSSs to redox reactions in operando, although the high

vacuum is still necessary¹³⁷. Luckily, routine angle-resolved experiments at near-ambient conditions might become the most advanced technologies in the long term. Invested with extra time and spin resolution, an in-situ inspection of catalytic spin transfer and further clarification of the effect of surface magnetism on heterogeneous catalytic reactions can be achieved¹⁵⁴⁻¹⁵⁶.

Another challenge is to find a TQM catalyst that is suitable for industrial-scale reactions. For hydrogen production and fuel cell reactions, the catalysts are expected to work on an industrial scale for a long time. Unfortunately, kinetic and stability assessments of most catalysis and conversion reactions focus on the low current densities (10 mA cm^{-2}) and potential ranges. Increasing the applied potential may destroy the surface of catalysts, or require high energy consumption that is far beyond what we can bear. Considering that both the charge and spin of electrons could be transported simultaneously for all the redox reactions, it is possible to boost the catalysis efficiency through the radical pair effects by manipulating spin polarization. Previous research has partially confirmed that the spin-polarized topological states can indeed interfere with the catalytic process directly^{8,157}, and most importantly, the spin polarization can be tuned by external fields such as current or magnetic fields^{158,159}. In the presence of a commercially permeated magnet, an improvement of 150 % in the OER current density can be obtained because of the polarized electrons in magnetic catalysts¹⁶⁰. Similarly, NbP family of WSMs exhibits a positive response at a magnetic field of 0.35 T. As hydrogen evolution catalysts, the efficiency is increased by 11 % for NbAs and 95 % for NbP¹⁶¹. More interestingly, the negative effects of surface oxidation and re-construction can be overcome as the spin properties can be reserved through the spin pinning effect¹⁵⁰. Although positive effects are reported in the presence of the magnetic field, we find that the intrinsic catalytic activities can be suppressed significantly, for example, the turnover frequency of topological semimetal Co_2MnGa is decreased by 33 % as HER catalysts¹⁵⁴. Thus, how the magnetic fields and spin polarization ‘talk’ with the chemical reactions requires more insightful exploration.

As for energy storage devices including the LIBs, NIBs, KIBs, and supercapacitors, the electrode materials are one of the most vital factors to realize the high specific

capacity, high energy density, and excellent cycling stability. TQMs with high electrical conductivity and desirable carrier mobility are the promising candidate electrode materials for these energy storage devices. Yet, the synthesis of promising topological electrode materials is another major challenge. Most of the topological batteries are still in theoretical perspective, synthetic condition even needs more efforts⁹⁹. Moreover, the fundamental knowledge such as the suitable voltage windows and the discharge voltage platform of different TQM electrode materials in the different energy storage devices is unclear yet. These issues need the considerable effort of researchers to be devoted. However, we are confident that in near future, except for these applications in this perspective, more and more new energy-related applications such as biomass conversion, nitrogen fixation will be attempted and achieved, in which chemists and physicists need to make joint efforts.

References:

- 1 Bernevig, B. A., Hughes, T. L. & Zhang, S.-C. Quantum spin hall effect and topological phase transition in HgTe quantum wells. *Science* **314**, 1757-1761 (2006).
- 2 Fu, L. & Kane, C. L. Topological insulators with inversion symmetry. *Phys. Rev. B* **76**, 045302 (2007).
- 3 Bradlyn, B. *et al.* Topological quantum chemistry. *Nature* **547**, 298-305 (2017).
- 4 Zhang, T. *et al.* Catalogue of topological electronic materials. *Nature* **566**, 475-479 (2019).
- 5 Liang, T. *et al.* Anomalous Nernst effect in the Dirac semimetal Cd₃As₂. *Phys. Rev. Lett.* **118**, 136601 (2017).
- 6 Vergniory, M. G. *et al.* A complete catalogue of high-quality topological materials. *Nature* **566**, 480-485 (2019).
- 7 Fu, C., Sun, Y. & Felser, C. Topological thermoelectrics. *APL Mater.* **8**, 040913

- (2020).
- 8 Rajamathi, C. R. *et al.* Photochemical water splitting by bismuth chalcogenide topological insulators. *ChemPhysChem* **18**, 2322-2327 (2017).
 - 9 He, Y. *et al.* Topological metal and noncentrosymmetric superconductor α -BiPd as an efficient candidate for the hydrogen evolution reaction. *Mater. Chem. Front.* **3**, 2184-2189 (2019).
 - 10 He, Y. *et al.* Topological type-II Dirac semimetal and superconductor PdTe₂ for ethanol electrooxidation. *Energy Technol.* **7**, 1900663 (2019).
 - 11 He, Y. *et al.* Discovery and facile synthesis of a new silicon based family as efficient hydrogen evolution reaction catalysts: a computational and experimental investigation of metal monosilicides. *Small* **17**, 2006153 (2021).
 - 12 Li, G. *et al.* Surface states in bulk single crystal of topological semimetal Co₃Sn₂S₂ toward water oxidation. *Sci. Adv.* **5**, eaaw9867 (2019).
 - 13 Li, G. *et al.* Dirac nodal arc semimetal PtSn₄: an ideal platform for understanding surface properties and catalysis for hydrogen evolution. *Angew. Chem. Int. Ed.* **58**, 13107-13112 (2019).
 - 14 Li, G. *et al.* In situ modification of a delafossite-type PdCoO₂ bulk single crystal for reversible hydrogen sorption and fast hydrogen evolution. *ACS Energy Lett.* **4**, 2185-2191 (2019).
 - 15 Li, G. & Felser, C. Heterogeneous catalysis at the surface of topological materials. *Appl. Phys. Lett.* **116**, 070501 (2020).
 - 16 Yang, Q. *et al.* Topological engineering of Pt-group-metal-based chiral crystals toward high-efficiency hydrogen evolution catalysts. *Adv. Mater.* **32**, 1908518 (2020).
 - 17 Tian, J., Hong, S., Miotkowski, I., Datta, S. & Chen, Y. P. Observation of current-induced, long-lived persistent spin polarization in a topological insulator: A rechargeable spin battery. *Sci. Adv.* **3**, e1602531 (2017).
 - 18 Baldomir, D. & Faílde, D. On behind the physics of the thermoelectricity of topological insulators. *Sci. Rep.* **9**, 6324 (2019).
 - 19 Singh, S., Kaur, K. & Kumar, R. Quest of thermoelectricity in topological

- insulators: A density functional theory study. *Appl. Surf. Sci.* **418**, 232-237 (2017).
- 20 Singh, S., Wu, Q., Yue, C., Romero, A. H. & Soluyanov, A. A. Topological phonons and thermoelectricity in triple-point metals. *Phys. Rev. Mater.* **2**, 114204 (2018).
- 21 Fu, C. *et al.* Large Nernst power factor over a broad temperature range in polycrystalline Weyl semimetal NbP. *Energy Environ. Sci.* **11**, 2813-2820 (2018).
- 22 Xu, Y. Thermoelectric effects and topological insulators. *Chin. Phys. B* **25**, 117309 (2016).
- 23 Heremans, J. P., Cava, R. J. & Samarth, N. Tetradymites as thermoelectrics and topological insulators. *Nat. Rev. Mater.* **2**, 17049 (2017).
- 24 Turner, J. A. Sustainable hydrogen production. *Science* **305**, 972-974 (2004).
- 25 Wang, X. *et al.* A metal-free polymeric photocatalyst for hydrogen production from water under visible light. *Nat. Mater.* **8**, 76-80 (2009).
- 26 Mahmood, J. *et al.* Encapsulating iridium nanoparticles inside a 3D cage like organic network as an efficient and durable catalyst for the hydrogen evolution reaction. *Adv. Mater.* **30**, 1805606 (2018).
- 27 Wang, F. *et al.* Technologies and perspectives for achieving carbon neutrality. *The Innovation* **2**, 100180 (2021).
- 28 Liu, W. *et al.* Single-site active cobalt-based photocatalyst with a long carrier lifetime for spontaneous overall water splitting. *Angew. Chem. Int. Ed.* **56**, 9312-9317 (2017).
- 29 Zhang, M., Guan, J., Tu, Y., Wang, S. & Deng, D. Highly efficient conversion of surplus electricity to hydrogen energy via polysulfides redox. *The Innovation* **2**, 100144 (2021).
- 30 Bai, S., Jiang, J., Zhang, Q. & Xiong, Y. Steering charge kinetics in photocatalysis: intersection of materials syntheses, characterization techniques and theoretical simulations. *Chem. Soc. Rev.* **44**, 2893-2939 (2015).
- 31 Dong, Y. *et al.* Enhanced catalytic performance of Pt by coupling with carbon defects. *The Innovation* **2**, 100161 (2021).
- 32 Luo, Y., Zhang, Z., Chhowalla, M. & Liu, B. Recent advances in design of

- electrocatalysts for high-current-density water splitting. *Adv. Mater.* **34**, 2108133 (2022).
- 33 Mistry, H., Varela, A. S., Köhl, S., Strasser, P. & Cuenya, B. R. Nanostructured electrocatalysts with tunable activity and selectivity. *Nat. Rev. Mater.* **1**, 16009 (2016).
- 34 Zhou, S. *et al.* Low-dimensional non-metal catalysts: principles for regulating p-orbital-dominated reactivity. *npj Comput. Mater.* **7**, 186 (2021).
- 35 Suntivich, J., May, K. J., Gasteiger, H. A., Goodenough, J. B. & Shao-Horn, Y. A perovskite oxide optimized for oxygen evolution catalysis from molecular orbital principles. *Science* **334**, 1383-1385 (2011).
- 36 Hasan, M. Z. & Kane, C. L. Colloquium: Topological insulators. *Rev. Mod. Phys.* **82**, 3045-3067 (2010).
- 37 Xiao, J., Kou, L., Yam, C.-Y., Frauenheim, T. & Yan, B. Toward rational design of catalysts supported on a topological insulator substrate. *ACS Catal.* **5**, 7063-7067 (2015).
- 38 Qu, Q. *et al.* Expediting hydrogen evolution through topological surface states on Bi₂Te₃. *ACS Catal.* **10**, 2656-2666 (2020).
- 39 Qu, Q. *et al.* Role of topological surface states and mirror symmetry in topological crystalline insulator SnTe as an efficient electrocatalyst. *Nanoscale* **13**, 18160-18172 (2021).
- 40 Li, L., Zeng, J., Qin, W., Cui, P. & Zhang, Z. Tuning the hydrogen activation reactivity on topological insulator heterostructures. *Nano Energy* **58**, 40-46 (2019).
- 41 Qu, Q., Liu, B., Sum Lau, W., Pan, D. & Keong Sou, I. Highly active hydrogen evolution facilitated by topological surface states on a Pd/SnTe metal/topological crystalline insulator heterostructure. Preprint at <https://arxiv.org/abs/2112.04753> (2021).
- 42 Edmonds, M. T. *et al.* Stability and surface reconstruction of topological insulator Bi₂Se₃ on exposure to atmosphere. *J. Phys. Chem. C* **118**, 20413-20419 (2014).
- 43 Kong, D. *et al.* Rapid surface oxidation as a source of surface degradation factor for Bi₂Se₃. *ACS Nano* **5**, 4698-4703 (2011).

- 44 Izadi, S. *et al.* Interface-Dominated Topological Transport in Nanograined Bulk Bi₂Te₃. *Small* **17**, 2103281 (2021).
- 45 Burkov, A. A. Topological semimetals. *Nat. Mater.* **15**, 1145-1148 (2016).
- 46 Yan, B. & Felser, C. Topological materials: Weyl semimetals. *Annu. Rev. Condens. Matter Phys.* **8**, 337-354 (2017).
- 47 Sarkar, S., Yang, J., Tan, L. Z., Rappe, A. M. & Kronik, L. Molecule-adsorbed topological insulator and metal surfaces: a comparative first-principles study. *Chem. Mater.* **30**, 1849-1855 (2018).
- 48 Politano, A. *et al.* Tailoring the surface chemical reactivity of transition-metal dichalcogenide PtTe₂ crystals. *Adv. Funct. Mater.* **28**, 1706504 (2018).
- 49 Rajamathi, C. R. *et al.* Weyl semimetals as hydrogen evolution catalysts. *Adv. Mater.* **33**, 2103730 (2021).
- 50 Shekhar, C. *et al.* Extremely large magnetoresistance and ultrahigh mobility in the topological Weyl semimetal candidate NbP. *Nat. Phys.* **11**, 645-649.
- 51 Hu, Huang, H., Zhou, S. & Duan, W. Type-II Dirac fermions in the PtSe₂ class of transition metal dichalcogenides. *Phys. Rev. B* **94**, 121117 (2016).
- 52 Li, Y. *et al.* Topological origin of the type-II Dirac fermions in PtSe₂. *Phys. Rev. Mater.* **1**, 074202 (2017).
- 53 Zhang, K. *et al.* Experimental evidence for type-II Dirac semimetal in PtSe₂. *Phys. Rev. B* **96**, 125102 (2017).
- 54 Yan, M. *et al.* Lorentz-violating type-II Dirac fermions in transition metal dichalcogenide PtTe₂. *Nat. Commun.* **8**, 257 (2017).
- 55 Huang, H., Fan, X., Singh, D. J. & Zheng, W. Modulation of hydrogen evolution catalytic activity of basal plane in monolayer platinum and palladium dichalcogenides. *ACS Omega* **3**, 10058-10065 (2018).
- 56 Liu, Z. K. *et al.* Discovery of a three-dimensional topological Dirac semimetal, Na₃Bi. *Science* **343**, 864-867 (2014).
- 57 Chen, C. *et al.* Robustness of topological order and formation of quantum well states in topological insulators exposed to ambient environment. *Proc. Natl. Acad. Sci.* **109**, 3694-3698 (2012).

- 58 Hu, C., Zhang, L. & Gong, J. Recent progress made in the mechanism comprehension and design of electrocatalysts for alkaline water splitting. *Energy Environ. Sci.* **12**, 2620-2645 (2019).
- 59 Jiang, W.-J., Tang, T., Zhang, Y. & Hu, J.-S. Synergistic modulation of non-precious-metal electrocatalysts for advanced water splitting. *Acc. Chem. Res.* **53**, 1111-1123 (2020).
- 60 Joshi, B., Thamizhavel, A. & Ramakrishnan, S. Superconductivity in noncentrosymmetric BiPd. *Phys. Rev. B* **84**, 064518 (2011).
- 61 Xu, R., Groot, R. A. d. & Lugt, W. v. d. The electrical resistivities of liquid Pd-Bi alloys and the band structure of crystalline β -PdBi₂ and PdBi. *J. Phys. Condens. Matter* **4**, 2389-2395 (1992).
- 62 Rajamathi, C. R. *et al.* Weyl semimetals as hydrogen evolution catalysts. *Adv. Mater.* **29**, 1606202 (2017).
- 63 Kong, X.-P. *et al.* Development of a Ni-doped VAl₃ topological semimetal with a significantly enhanced her catalytic performance. *J. Phys. Chem. Lett.* **12**, 3740-3748 (2021).
- 64 He, Y. *et al.* Topologically nontrivial 1T'-MoTe₂ as highly efficient hydrogen evolution electrocatalyst. *J. Phys. Mater.* **4**, 014001 (2020).
- 65 Sun, Y., Wu, S.-C., Ali, M. N., Felser, C. & Yan, B. Prediction of Weyl semimetal in orthorhombic MoTe₂. *Phys. Rev. B* **92**, 161107 (2015).
- 66 Xu, Y., Zhang, F. & Zhang, C. Structured Weyl points in spin-orbit coupled fermionic superfluids. *Phys. Rev. Lett.* **115**, 265304, (2015).
- 67 Huang, L. *et al.* Spectroscopic evidence for a type II Weyl semimetallic state in MoTe₂. *Nat. Mater.* **15**, 1155-1160 (2016).
- 68 Deng, K. *et al.* Experimental observation of topological Fermi arcs in type-II Weyl semimetal MoTe₂. *Nat. Phys.* **12**, 1105-1110 (2016).
- 69 Jiang, J. *et al.* Signature of type-II Weyl semimetal phase in MoTe₂. *Nat. Commun.* **8**, 13973 (2017).
- 70 Qian, X., Liu, J., Fu, L. & Li, J. Quantum spin Hall effect in two-dimensional transition metal dichalcogenides. *Science* **346**, 1344-1347 (2014).

- 71 Song, P. *et al.* Few-layer 1T' MoTe₂ as gapless semimetal with thickness dependent carrier transport. *2D Mater.* **5**, 031010 (2018).
- 72 Hammer, B. & Norskov, J. K. Why gold is the noblest of all the metals. *Nature* **376**, 238-240 (1995).
- 73 Ritz, R. *et al.* Formation of a topological non-Fermi liquid in MnSi. *Nature* **497**, 231-234 (2013).
- 74 Tang, P., Zhou, Q. & Zhang, S.-C. Multiple types of topological fermions in transition metal silicides. *Phys. Rev. Lett.* **119**, 206402 (2017).
- 75 Yuan, Q.-Q. *et al.* Quasiparticle interference evidence of the topological Fermi arc states in chiral fermionic semimetal CoSi. *Sci. Adv.* **5**, eaaw9485 (2019).
- 76 Sanchez, D. S. *et al.* Topological chiral crystals with helicoid-arc quantum states. *Nature* **567**, 500-505 (2019).
- 77 Li, J. *et al.* Topological quantum catalyst: Dirac nodal line states and a potential electrocatalyst of hydrogen evolution in the TiSi family. *Sci. China Mater.* **61**, 23-29 (2018).
- 78 Changdar, S. *et al.* Electronic structure studies of FeSi: A chiral topological system. *Phys. Rev. B* **101**, 235105 (2020).
- 79 Schröter, N. B. M. *et al.* Observation and control of maximal Chern numbers in a chiral topological semimetal. *Science* **369**, 179-183 (2020).
- 80 Narang, P., Garcia, C. A. C. & Felser, C. The topology of electronic band structures. *Nature Materials* **20**, 293-300 (2021).
- 81 Liu, W. *et al.* Theoretical realization of hybrid Weyl state and associated high catalytic performance for hydrogen evolution in NiSi. *iScience* **25**, 103543 (2022).
- 82 Suntivich, J. *et al.* Design principles for oxygen-reduction activity on perovskite oxide catalysts for fuel cells and metal–air batteries. *Nat. Chem.* **3**, 546-550 (2011).
- 83 Yu, M. *et al.* Tunable *eg* Orbital occupancy in Heusler compounds for oxygen evolution reaction. *Angew. Chem. Int. Ed.* **60**, 5800-5805 (2021).
- 84 Sun, J. *et al.* Carbon nanorings and their enhanced lithium storage properties. *Adv. Mater.* **25**, 1125-1130 (2013).
- 85 Liu, H. *et al.* Porous Carbon composites for next generation rechargeable lithium

- batteries. *Adv. Energy Mater.* **7**, 1700283 (2017).
- 86 Fu, A. *et al.* Recent advances in hollow porous carbon materials for lithium–sulfur batteries. *Small* **15**, 1804786 (2019).
- 87 Liu, J., Wang, S. & Sun, Q. All-carbon-based porous topological semimetal for Li-ion battery anode material. *Proc. Natl. Acad. Sci.* **114**, 651 (2017).
- 88 Xie, H., Qie, Y., Imran, M. & Sun, Q. Topological semimetal porous carbon as a high-performance anode for Li-ion batteries. *J. Mater. Chem. A* **7**, 14253-14259 (2019).
- 89 Wang, J.-T. *et al.* Body-Centered Orthorhombic C₁₆: A Novel Topological Node-Line Semimetal. *Phys. Rev. Lett.* **116**, 195501 (2016).
- 90 Qie, Y., Liu, J., Wang, S., Sun, Q. & Jena, P. Tetragonal C₂₄: a topological nodal-surface semimetal with potential as an anode material for sodium ion batteries. *J. Mater. Chem. A* **7**, 5733-5739 (2019).
- 91 Yi, X. *et al.* Topological dual double node-line semimetals NaAlSi(Ge) and their potential as cathode material for sodium ion batteries. *J. Mater. Chem. C* **7**, 15375-15381 (2019).
- 92 Wang, J.-T., Weng, H. & Chen, C. Topological nodal line semimetals in graphene network structures. *Adv. Phys. X* **4**, 1625724 (2019).
- 93 Chen, Y., Xie, Y., Yan, X., Cohen, M. L. & Zhang, S. Topological carbon materials: A new perspective. *Phys. Rep.* **868**, 1-32 (2020).
- 94 Liu, J., Li, X., Wang, Q., Kawazoe, Y. & Jena, P. A new 3D Dirac nodal-line semimetallic graphene monolith for lithium ion battery anode materials. *J. Mater. Chem. A* **6**, 13816-13824 (2018).
- 95 Zhou, T. *et al.* Enhanced sodium-ion battery performance by structural phase transition from two-dimensional hexagonal-SnS₂ to orthorhombic-SnS. *ACS Nano* **8**, 8323-8333 (2014).
- 96 Ma, C. *et al.* Investigating the energy storage mechanism of SnS₂-rGO composite anode for advanced Na-ion batteries. *Chem. Mater.* **27**, 5633-5640 (2015).
- 97 Kim, H. *et al.* Recent progress in electrode materials for sodium-ion batteries. *Adv. Energy Mater.* **6**, 1600943 (2016).

- 98 Feng, X. *et al.* Monoclinic C₁₆: sp²-sp³ hybridized nodal-line semimetal protected by PT-symmetry. *Carbon* **127**, 527-532 (2018).
- 99 Liu, J., Wang, S., Qie, Y., Zhang, C. & Sun, Q. High-pressure-assisted design of porous topological semimetal carbon for Li-ion battery anode with high-rate performance. *Phys. Rev. Mater.* **2**, 025403 (2018).
- 100 Shen, Y., Wang, Q., Kawazoe, Y. & Jena, P. Potential of porous nodal-line semi-metallic carbon for sodium-ion battery anode. *J. Power Sources* **478**, 228746 (2020).
- 101 Qie, Y. *et al.* Interpenetrating silicene networks: A topological nodal-line semimetal with potential as an anode material for sodium ion batteries. *Phys. Rev. Mater.* **2**, 084201 (2018).
- 102 Gao, Y. *et al.* Hexagonal supertetrahedral boron: A topological metal with multiple spin-orbit-free emergent fermions. *Phys. Rev. Mater.* **3**, 044202 (2019).
- 103 Xie, H., Qie, Y., Muhammad, I. & Sun, Q. B₄ Cluster-based 3D porous topological metal as an anode material for both Li- and Na-ion batteries with a superhigh capacity. *J. Phys. Chem. Lett.* **12**, 1548-1553 (2021).
- 104 Liu, X. *et al.* Exploring sodium storage mechanism of topological insulator Bi₂Te₃ nanosheets encapsulated in conductive polymer. *Energy Storage Mater.* **41**, 255-263 (2021).
- 105 Soares, D. M. & Singh, G. Weyl semimetal orthorhombic T_d-WTe₂ as an electrode material for sodium- and potassium-ion batteries. *Nanotechnology* **32**, 505402 (2021).
- 106 Chang, T.-R. *et al.* Type-II symmetry-protected topological Dirac semimetals. *Phys. Rev. Lett.* **119**, 026404 (2017).
- 107 Sottmann, J. *et al.* How crystallite size controls the reaction path in nonaqueous metal ion batteries: the example of sodium bismuth alloying. *Chem. Mater.* **28**, 2750-2756 (2016).
- 108 Chiu, W.-C. *et al.* Topological Dirac semimetal phase in bismuth based anode materials for sodium-ion batteries. *Condens. Matter* **5**, 39 (2020).
- 109 Lv, B. Q., Qian, T. & Ding, H. Experimental perspective on three-dimensional

- topological semimetals. *Rev. Mod. Phys.* **93**, 025002 (2021).
- 110 Wu, W. & Sun, Q. Screening Topological quantum materials for Na-ion battery cathode. *ACS Mater. Lett.* **4**, 175-180 (2022).
- 111 Tang, F., Po, H. C., Vishwanath, A. & Wan, X. Comprehensive search for topological materials using symmetry indicators. *Nature* **566**, 486-489 (2019).
- 112 Li, X., Liu, J., Wang, F. Q., Wang, Q. & Jena, P. Rational design of porous nodal-line semimetallic carbon for K-ion battery anode materials. *J. Phys. Chem. Lett.* **10**, 6360-6367 (2019).
- 113 Zhang, Q. *et al.* Issues and rational design of aqueous electrolyte for Zn-ion batteries. *SusMat* **1**, 432-447 (2021).
- 114 Zhao, Y. *et al.* Vacancy modulating $\text{Co}_3\text{Sn}_2\text{S}_2$ topological semimetal for aqueous Zinc-ion batteries. *Angew. Chem. Int. Ed.* **61**, e202111826 (2022).
- 115 Yu, P. *et al.* Controllable synthesis of atomically thin type-II Weyl semimetal WTe_2 nanosheets: an advanced electrode material for all-solid-state flexible supercapacitors. *Adv. Mater.* **29**, 1701909 (2017).
- 116 Kumar, D. R., Nguyen, T. T., Lamiel, C. & Shim, J.-J. Layered 2-D Bi_2Se_3 nanosheets intercalated by $\text{Ni}(\text{OH})_2$ and their supercapacitor performance. *Mater. Lett.* **165**, 257-262 (2016).
- 117 Yang, J. *et al.* Integrated quasiplane heteronanostructures of $\text{MoSe}_2/\text{Bi}_2\text{Se}_3$ hexagonal nanosheets: synergetic electrocatalytic water splitting and enhanced supercapacitor performance. *Adv. Funct. Mater.* **27**, 1703864 (2017).
- 118 Soluyanov, A. A. *et al.* Type-II Weyl semimetals. *Nature* **527**, 495-498 (2015).
- 119 König, M. *et al.* Quantum spin hall insulator state in hgte quantum wells. *Science* **318**, 766-770 (2007).
- 120 Bruno, F. Y. *et al.* Observation of large topologically trivial Fermi arcs in the candidate type-II Weyl semimetal WTe_2 . *Phys. Rev. B* **94**, 121112 (2016).
- 121 Feng, B. *et al.* Spin texture in type-II Weyl semimetal WTe_2 . *Phys. Rev. B* **94**, 195134 (2016).
- 122 Chen, H., Zhu, W., Xiao, D. & Zhang, Z. CO oxidation facilitated by robust surface states on Au-covered topological insulators. *Phys. Rev. Lett.* **107**, 056804 (2011).

- 123 Tang, M., Shen, H., Xie, H. & Sun, Q. Metal-free catalyst B₂S sheet for effective CO₂ electrochemical reduction to CH₃OH. *ChemPhysChem* **21**, 779-784 (2020).
- 124 Zhu, X., Wang, Y., Jing, Y., Heine, T. & Li, Y. β-PdBi₂ monolayer: two-dimensional topological metal with superior catalytic activity for carbon dioxide electroreduction to formic acid. *Mater. Today Adv.* **8**, 100091 (2020).
- 125 Kojima, T., Kameoka, S., Fujii, S., Ueda, S. & Tsai, A.-P. Catalysis-tunable Heusler alloys in selective hydrogenation of alkynes: A new potential for old materials. *Sci. Adv.* **4**, eaat6063 (2018).
- 126 Prinz, J. *et al.* Adsorption of small hydrocarbons on the three-fold PdGa surfaces: the road to selective hydrogenation. *J. Am. Chem. Soc.* **136**, 11792-11798 (2014).
- 127 He, Q. L., Lai, Y. H., Lu, Y., Law, K. T. & Sou, I. K. Surface reactivity enhancement on a Pd/Bi₂Te₃ heterostructure through robust topological surface states. *Sci. Rep.* **3**, 2497 (2013).
- 128 Xie, H. *et al.* Facet engineering to regulate surface states of topological crystalline insulator bismuth rhombic dodecahedrons for highly energy efficient electrochemical CO₂ reduction. *Adv. Mater.* **33**, 2008373 (2021).
- 129 Wang, J., Fan, C. Y., Jacobi, K. & Ertl, G. The kinetics of CO oxidation on RuO₂(110): bridging the pressure gap. *J. Phys. Chem. B* **106** (2002).
- 130 Wang, H. & Schneider, W. F. Adsorption and reactions of NO_x on RuO₂(110). *Catal. Today* **165**, 49-55 (2011).
- 131 Li, L., Qu, L., Cheng, J., Li, J. & Hao, Z. Oxidation of nitric oxide to nitrogen dioxide over Ru catalysts. *Appl. Catal. B Environ.* **88**, 224-231 (2009).
- 132 Radjenovic, J. *et al.* Electrochemical oxidation of trace organic contaminants in reverse osmosis concentrate using RuO₂/IrO₂-coated titanium anodes. *Water Res.* **45**, 1579-1586 (2011).
- 133 Song, S. & Jiang, S. Selective catalytic oxidation of ammonia to nitrogen over CuO/CNTs: The promoting effect of the defects of CNTs on the catalytic activity and selectivity. *Appl. Catal. B Environ.* **117-118**, 346-350 (2012).
- 134 Nelson, J. N. *et al.* Dirac nodal lines protected against spin-orbit interaction in IrO₂. *Phys. Rev. Mater.* **3**, 064205 (2019).

- 135 Sun, Y., Zhang, Y., Liu, C.-X., Felser, C. & Yan, B. Dirac nodal lines and induced spin Hall effect in metallic rutile oxides. *Phys. Rev. B* **95**, 235104 (2017).
- 136 Jovic, V. *et al.* Dirac nodal lines and flat-band surface state in the functional oxide RuO₂. *Phys. Rev. B* **98**, 241101 (2018).
- 137 Jovic, V. *et al.* Momentum for Catalysis: How surface reactions shape the RuO₂ flat surface state. *ACS Catal.* **11**, 1749-1757 (2021).
- 138 Yu, R., Weng, H., Fang, Z., Dai, X. & Hu, X. Topological Node-line semimetal and Dirac semimetal state in antiperovskite Cu₃PdN. *Phys. Rev. Lett.* **115**, 036807 (2015).
- 139 Wang, X., Chen, J. & Xie, D. Prospect of node-line semimetal Cu₃PdN to be a topological superconductor. *J. Supercond. Nov. Magn.* **30**, 2727-2734 (2017).
- 140 Jia, J., Hao, X., Chang, Y., Jia, M. & Wen, Z. Rational design of Cu₃PdN nanocrystals for selective electroreduction of carbon dioxide to formic acid. *J. Colloid Interface Sci.* **586**, 491-497 (2021).
- 141 Vaughn Li, D. D. *et al.* Solution synthesis of Cu₃PdN nanocrystals as ternary metal nitride electrocatalysts for the oxygen reduction reaction. *Chem. Mater.* **26**, 6226-6232 (2014).
- 142 Feng, B. *et al.* Experimental realization of two-dimensional Dirac nodal line fermions in monolayer Cu₂Si. *Nat. Commun.* **8**, 1007 (2017).
- 143 Yang, L.-M. *et al.* Two-dimensional Cu₂Si monolayer with planar hexacoordinate copper and silicon bonding. *J. Am. Chem. Soc.* **137**, 2757-2762 (2015).
- 144 Tang, M., Shen, H., Qie, Y., Xie, H. & Sun, Q. Edge-state-enhanced CO₂ electroreduction on topological Nodal-line semimetal Cu₂Si nanoribbons. *J. Phys. Chem. C* **123**, 2837-2842 (2019).
- 145 Hui, T. *et al.* Atmosphere induced amorphous and permeable carbon layer encapsulating PtGa catalyst for selective cinnamaldehyde hydrogenation. *J. Catal.* **389**, 229-240 (2020).
- 146 Ebrahimian, A. & Dadsetani, M. Alkali-metal-induced topological nodal line semimetal in layered XN₂ (X = Cr, Mo, W). *Front. Phys.* **13**, 137309 (2018).
- 147 Ma, L.-J. & Sun, Q. A topological semimetal Li₂CrN₂ sheet as a promising

- hydrogen storage material. *Nanoscale* **12**, 12106-12113 (2020).
- 148 Hu, D. *et al.* Green CO₂-assisted synthesis of mono- and bimetallic Pd/Pt nanoparticles on porous carbon fabricated from sorghum for highly selective hydrogenation of furfural. *ACS Sustain. Chem. Eng.* **7**, 15339-15345 (2019).
- 149 Wang, A. *et al.* Selective production of γ -valerolactone and valeric acid in one-pot bifunctional metal catalysts. *ChemistrySelect* **3**, 1097-1101 (2018).
- 150 Qiao, Y. *et al.* Preparation of SBA-15 supported Pt/Pd bimetallic catalysts using supercritical fluid reactive deposition: how do solvent effects during material synthesis affect catalytic properties? *Green Chem.* **19**, 977-986 (2017).
- 151 Xu, Y. *et al.* High-throughput calculations of magnetic topological materials. *Nature* **586**, 702-707 (2020).
- 152 Chen, X.-Q., Liu, J. & Li, J. Topological phononic materials: Computation and data. *The Innovation* **2**, 100134 (2021).
- 153 Katz, R. J., Zhu, Y., Mao, Z. & Schaak, R. E. Persistence and evolution of materials features during catalysis using topological and trivial polymorphs of MoTe₂. *ChemCatChem* **14**, e202101714 (2022).
- 154 Chen, Y. *et al.* Recent advances in topological quantum materials by angle-resolved photoemission spectroscopy. *Matter* **3**, 1114-1141 (2020).
- 155 Cuxart, M. G. *et al.* Molecular approach for engineering interfacial interactions in magnetic/topological insulator heterostructures. *ACS Nano* **14**, 6285-6294 (2020).
- 156 Kim, Y. & Lee, J. Time-resolved photoemission of infinitely periodic atomic arrangements: correlation-dressed excited states of solids. *npj Comput. Mater.* **6**, 132 (2020).
- 157 Wang, P. *et al.* Intrinsic magnetic topological insulators. *The Innovation* **2**, 100098 (2021).
- 158 Li, C. H., van 't Erve, O. M. J., Rajput, S., Li, L. & Jonker, B. T. Direct comparison of current-induced spin polarization in topological insulator Bi₂Se₃ and InAs Rashba states. *Nat. Commun.* **7**, 13518 (2016).
- 159 Pershoguba, S. S. & Yakovenko, V. M. Spin-polarized tunneling current through a thin film of a topological insulator in a parallel magnetic field. *Phys. Rev. B* **86**,

- 165404 (2012).
- 160 Garcés-Pineda, F. A., Blasco-Ahicart, M., Nieto-Castro, D., López, N. & Galán-Mascarós, J. R. Direct magnetic enhancement of electrocatalytic water oxidation in alkaline media. *Nat. Energy* **4**, 519-525 (2019).
- 161 Gupta, U. *et al.* Effect of magnetic field on the hydrogen evolution activity using non-magnetic Weyl semimetal catalysts. *Dalton Trans.* **49**, 3398-3402 (2020).
- 162 Wu, T. *et al.* Spin pinning effect to reconstructed oxyhydroxide layer on ferromagnetic oxides for enhanced water oxidation. *Nat. Commun.* **12**, 3634 (2021).
- 163 Li, G. *et al.* Carbon-tailored semimetal MoP as an efficient hydrogen evolution electrocatalyst in both alkaline and acid media. *Adv. Energy Mater.* **8**, 1801258 (2018).
- 164 Li, J. *et al.* Enhanced electrocatalytic hydrogen evolution from large-scale, facile-prepared, highly crystalline WTe₂ nanoribbons with Weyl semimetallic phase. *ACS Appl. Mater. Interfaces* **10**, 458-467 (2018).
- 165 Mc Manus, J. B. *et al.* Low-temperature synthesis and electrocatalytic application of large-area PtTe₂ thin films. *Nanotechnology* **31**, 375601 (2020).
- 166 Huang, K. *et al.* NiPS₃ quantum sheets modified nitrogen-doped mesoporous carbon with boosted bifunctional oxygen electrocatalytic performance. *J. Mater. Sci. . Technol.* **65**, 1-6 (2021).
167. Ni, Z. *et al.* Giant topological longitudinal circular photo-galvanic effect in the chiral multifold semimetal CoSi. *Nat. Commun.* **12**, 154 (2021).
- 168 Qi, X.-L. & Zhang, S.-C. Topological insulators and superconductors. *Rev. Mod. Phys.* **83**, 1057-1110 (2011).
- 169 Langmuir, I. The adsorption of gases on plane surfaces of glass, mica and platinum. *J. Am. Chem. Soc.* **40**, 1361-1403 (1918).
- 170 Hammer, B. & Norskov, J. K. Why gold is the noblest of all the metals. *Nature* **376**, 238-240 (1995).
- 171 Hwang, J. *et al.* Perovskites in catalysis and electrocatalysis. *Science* **358**, 751-756 (2017).

- 172 Yuan, Y. *et al.* Co₃Mo₃N—An efficient multifunctional electrocatalyst. *The Innovation* **2**, 100096 (2021).
- 173 Zhong, W. *et al.* Electronic Spin Moment As a Catalytic Descriptor for Fe Single-Atom Catalysts Supported on C₂N. *J. Am. Chem. Soc.* **143**, 4405-4413 (2021).
- 174 Bielański, A., Dereń, J. & Haber, J. Electric conductivity and catalytic activity of semiconducting oxide catalysts. *Nature* **179**, 668-669 (1957).
- 175 Yun, T. G., Heo, Y., Bin Bae, H. & Chung, S.-Y. Elucidating intrinsic contribution of d-orbital states to oxygen evolution electrocatalysis in oxides. *Nat. Commun.* **12**, 824 (2021).
- 176 Liu, L. & Corma, A. Confining isolated atoms and clusters in crystalline porous materials for catalysis. *Nat. Rev. Mater.* **6**, 244-263 (2021).
- 177 Bi, W. *et al.* Molecular co-catalyst accelerating hole transfer for enhanced photocatalytic H₂ evolution. *Nat. Commun.* **6**, 8647 (2015).
- 178 Tong, Y. *et al.* Spin-state regulation of perovskite cobaltite to realize enhanced oxygen evolution activity. *Chem* **3**, 812-821 (2017).
- 179 Rodgers, C. T. & Hore, P. J. Chemical magnetoreception in birds: The radical pair mechanism. *Pro. Natl. Acad. Sci.* **106**, 353-360 (2009).

Acknowledgments

This work is supported by the National Natural Science Foundation of China (11922415, 22078374, 21776324), Guangdong Basic and Applied Basic Research Foundation (2022A1515011168, 2019A1515011718, 2019B1515120058, 2020A1515011149), Key Research & Development Program of Guangdong Province, China (2019B110209003), the Pearl River Scholarship Program of Guangdong Province Universities and Colleges (20191001) and Hundred Talent Plan from Sun Yat-sen University, and the Foundation of President of Ningbo Institute of Materials Technology and Engineering (NIMTE) of the Chinese Academy of Sciences (CAS).

Author contributions

H. Luo is the leading author in organizing this perspective. All authors occupy the writing and polish the manuscript.

Competing interests

The authors declare no competing interests.

Peer review information

Nature Reviews Physics thanks Ankita Anirban and the other, anonymous, reviewer for their contribution to the peer review of this review.

Publisher's note

Springer Nature remains neutral with regard to jurisdictional claims in published maps and institutional affiliations.

Table 1

Table 1 | HER and OER performance for various topological quantum materials (TQMs), where the TIs, TSMs, and TSCs represent the topological insulators, topological semimetal, and topological superconductor, respectively.

Water splitting							
Applications	TQMs	Compounds	Conductivity (σ)/mobility (μ) value at room temperature	Morphology	η_{10} mA cm ⁻² (mV)	Tafel slope (mV dec ⁻¹)	Stability
HER	TIs	Pd/SnTe (REF. ⁴¹)	$\sigma_{\text{SnTe}} = 8.06 \times 10^3 \text{ S}\cdot\text{cm}^{-1}$ $\mu_{\text{SnTe}} = 46 \text{ cm}^2\cdot\text{V}^{-1} \text{ s}^{-1}$	Metal/TI Heterostructure	86	29.14	1000 CV cycles
		Bi ₂ Te ₃ (REF. ³⁸)	$\sigma = 1.22 \times 10^3 \text{ S}\cdot\text{cm}^{-1}$ $\mu = 28 \text{ cm}^2\cdot\text{V}^{-1} \text{ s}^{-1}$	Thin film	219	47.87	48 h at 10 mA cm ⁻¹
		Bi ₂ Te ₃ (REF. ⁴⁴)	$\mu > 10^3 \text{ cm}^2 \text{ V}^{-1} \text{ s}^{-1}$	nanoparticles	-	-	-
	TSMs	NbP (REF. ⁶²)		Single crystal	3520 $\mu\text{mol g}^{-1}$	-	-

			$\sigma = 6.30 \times 10^5 \text{ S}\cdot\text{cm}^{-1}$		¹ for 6.3 h	
	NbP (REF. ⁶¹)		$\mu = 2.75 \times 10^2 \text{ cm}^2\cdot\text{V}^{-1} \text{ s}^{-1}$	Single crystal powder	7442 $\mu\text{mol g}^{-1}$ for 6 h	-
	NbP (REF. ¹⁶⁰)			Single crystal powder	333 $\mu\text{mol g}^{-1}$ for 3 h	-
	TiSi (REF. ¹¹)		$\sigma = 3.23 \times 10^4 \text{ S}\cdot\text{cm}^{-1}$	Polycrystal	34	27.1
	MnSi (REF. ¹¹)		$\sigma = 8.17 \times 10^3 \text{ S}\cdot\text{cm}^{-1}$	Polycrystal	39	27.3
	FeSi (REF. ¹¹)		$\sigma = 2.6 \times 10^4 \text{ S}\cdot\text{cm}^{-1}$	Polycrystal	42	29.7
	RuSi (REF. ¹¹)		$\sigma = 1.11 \times 10^2 \text{ S}\cdot\text{cm}^{-1}$	Polycrystal	42	23.6
	NiSi (REF. ¹¹)		$\sigma = 9.65 \times 10^4 \text{ S}\cdot\text{cm}^{-1}$	Polycrystal	43	30.1
	CoSi (REF. ¹¹)		$\sigma = 7.47 \times 10^3 \text{ S}\cdot\text{cm}^{-1}$ $\mu = 119 \text{ cm}^2\cdot\text{V}^{-1} \text{ s}^{-1}$	Polycrystal	54	31.5
	RhSi (REF. ¹¹)		$\sigma = 3.61 \times 10^3 \text{ S}\cdot\text{cm}^{-1}$	Polycrystal	114	50.8
	1T'-MoTe ₂ (REF. ⁶⁴)		$\sigma = 1.91 \times 10^3 \text{ S}\cdot\text{cm}^{-1}$ $\mu = 16.2 \text{ cm}^2\cdot\text{V}^{-1} \text{ s}^{-1}$	Bulk form	356	127
	PtTe ₂ (REF. ⁴⁸)		$\sigma = 3.3 \times 10^6 \text{ S}\cdot\text{cm}^{-1}$ $\mu = 4.41 \times 10^2 \text{ cm}^2\cdot\text{V}^{-1} \text{ s}^{-1}$	Layered bulk form	540	110
	MoP (REF. ¹⁶³)		$\sigma = 4.30 \times 10^5 \text{ S}\cdot\text{cm}^{-1}$ $\mu = 2.32 \times 10^3 \text{ cm}^2\cdot\text{V}^{-1} \text{ s}^{-1}$	Nanocrystals	154	102
	WTe ₂ (REF. ¹⁶⁴)		$\sigma = 7.41 \times 10^2 \text{ S}\cdot\text{cm}^{-1}$ $\mu = 84.21 \text{ cm}^2\cdot\text{V}^{-1} \text{ s}^{-1}$	Nanoribbons	430	57
	PdGa (REF. ¹⁶)		$\sigma = 6.67 \times 10^4 \text{ S}\cdot\text{cm}^{-1}$	Single crystal	207	120
	RhSi (REF. ¹⁶)		$\sigma = 3.61 \times 10^3 \text{ S}\cdot\text{cm}^{-1}$	Single crystal	280	145
	PtGa (REF. ¹⁶)		$\sigma = 1.08 \times 10^4 \text{ S}\cdot\text{cm}^{-1}$	Single crystal	13.3	16
	PtAl (REF. ¹⁶)		-	Polycrystalline ingot	14	20
						100 h at different

							overpotential
		PtSn ₄ (REF. ¹³)	$\sigma = 1.27 \times 10^2 \text{ S}\cdot\text{cm}^{-1}$ $\mu = 200 \text{ cm}^2\cdot\text{V}^{-1} \text{ s}^{-1}$	Single crystal	37	39	400 h at 46 mV
		PtTe ₂ (REF. ¹⁶⁵)	$\sigma = 3.3 \times 10^6 \text{ S}\cdot\text{cm}^{-1}$ $\mu = 4.41 \times 10^2 \text{ cm}^2\cdot\text{V}^{-1} \text{ s}^{-1}$	Thin film	330	85	-
		1T'-MoTe ₂ (REF. ⁶⁴)	$\sigma = 1 \times 10^3 \text{ S}\cdot\text{cm}^{-1}$ $\mu = \times 10^2 \text{ cm}^2\cdot\text{V}^{-1} \text{ s}^{-1}$	Single crystal	73	46.3	10 h
		VAl ₃ (REF. ⁶³)	$\sigma = 8.64 \times 10^3 \text{ S}\cdot\text{cm}^{-1}$ $\mu = 1.31 \times 10^2 \text{ cm}^2\cdot\text{V}^{-1} \text{ s}^{-1}$	Microscale single crystals	319	68	-
		V _{0.75} Ni _{0.25} A l ₃ (REF. ⁶³)	$\mu = 4.67 \text{ cm}^2\cdot\text{V}^{-1} \text{ s}^{-1}$	Microscale single crystals	175	73	30 h at 200 mV
	Possible TSCs	PdTe ₂ (REF. ¹⁰)	$\sigma = 4.30 \times 10^6 \text{ S}\cdot\text{cm}^{-1}$ $\mu = 1.19 \times 10^3 \text{ cm}^2\cdot\text{V}^{-1} \text{ s}^{-1}$	Layered bulk form	740	92	-
		α -BiPd (REF. ⁹)	$\sigma = 2.10 \times 10^4 \text{ S}\cdot\text{cm}^{-1}$	Nanosheets	144	104	13 h at 500 mV
OER	TSMs	Co ₃ Sn ₂ S ₂ (REF. ¹²)	$\sigma = 2.68 \times 10^3 \text{ S}\cdot\text{cm}^{-1}$ $\mu = 2.6 \times 10^3 \text{ cm}^2\cdot\text{V}^{-1} \text{ s}^{-1}$	Single crystal	300	74	12 h at 1.497 mV
		Co ₂ MnAl (REF. ⁸³)	$\sigma = 4.12 \times 10^3 \text{ S}\cdot\text{cm}^{-1}$	Crystal	-	68	-
		Co ₂ MnGa (REF. ⁸³)	$\sigma = 5.77 \times 10^3 \text{ S}\cdot\text{cm}^{-1}$	Crystal	-	67	12 h at 1.63 V
		NiPS ₃ (REF. ¹⁶⁶)	$\sigma = 1 \times 10^{-7} \text{ S}\cdot\text{cm}^{-1}$ $\mu = 3.5 \text{ cm}^2\cdot\text{V}^{-1} \text{ s}^{-1}$	Nano sheets	301	43	20 h at 10 mA cm ⁻²

Table 2

Table 2 | Batteries and supercapacitors performance for various topological quantum materials (TQMs), where the TIs, TSMs, and TSCs represent the topological insulators, topological semimetal, and topological superconductor, respectively.

Battery/ Supercapacitors							
Applications	TQMs	Compounds	Conductivity (σ)/mobility (μ) value at room temperature	Morphology	Specific capacity (mAh g ⁻¹)	Maximum energy density (Wh kg ⁻¹)	Stability
LIBs	TSMs	bco-C16 (REF. ⁸⁷)	-	Bulk form	558	-	-
		HZMG-42 (REF. ⁹⁴)	$\sigma = 1 \times 10^{-6}$ S·cm ⁻¹	Bulk form	638	-	-
		m-C16 (REF. ⁸⁸)	-	Bulk form	558	-	-
NIBs	TSMs	tC24 (REF. ⁹⁰)	-	Bulk form	233	-	-
		T _d -WTe ₂ (REF. ¹⁰⁵)	$\sigma = 7.41 \times 10^2$ S·cm ⁻¹ $\mu = 84.21$ cm ² ·V ⁻¹ s ⁻¹	Layered bulk form	245 (0.1 A g ⁻¹)	-	-
		NaAlSi (REF. ⁹¹)	$\sigma = 6.02 \times 10^2$ S·cm ⁻¹	-	476	-	-
		NaAlGe (REF. ⁹¹)	-	-	238	-	-
KIBs	TSMs	T _d -WTe ₂ (REF. ¹⁰⁵)	$\sigma = 7.41 \times 10^2$ S·cm ⁻¹ $\mu = 84.21$ cm ² ·V ⁻¹ s ⁻¹	Layered bulk form	238 (0.1 A g ⁻¹)	-	-
ZIBs	TSMs	Co ₃ Sn ₂ S ₂ (REF. ¹¹⁴)	$\sigma = 2.68 \times 10^3$ S·cm ⁻¹ $\mu = 2.6 \times 10^3$ cm ² ·V ⁻¹ s ⁻¹	Crystal pellets	160 (1 A g ⁻¹)	305 (0.2 A g ⁻¹)	1460 cycles at 1 A g ⁻¹
Supercapacitors							
Applications	TQMs	Compounds	Conductivity (σ)/mobility (μ) value at room temperature	Morphology	Specific mass capacitance (F g ⁻¹)	Maximum energy density (Wh kg ⁻¹)	Stability
Supercapacitors	TSMs	T _d -WTe ₂ (REF. ¹¹⁵)	$\sigma = 7.41 \times 10^2$ S·cm ⁻¹ $\mu = 84.21$ cm ² ·V ⁻¹ s ⁻¹	Thin film	221 (1 A g ⁻¹)	31	5500 cycles at 3.4 A cm ⁻³

Figures

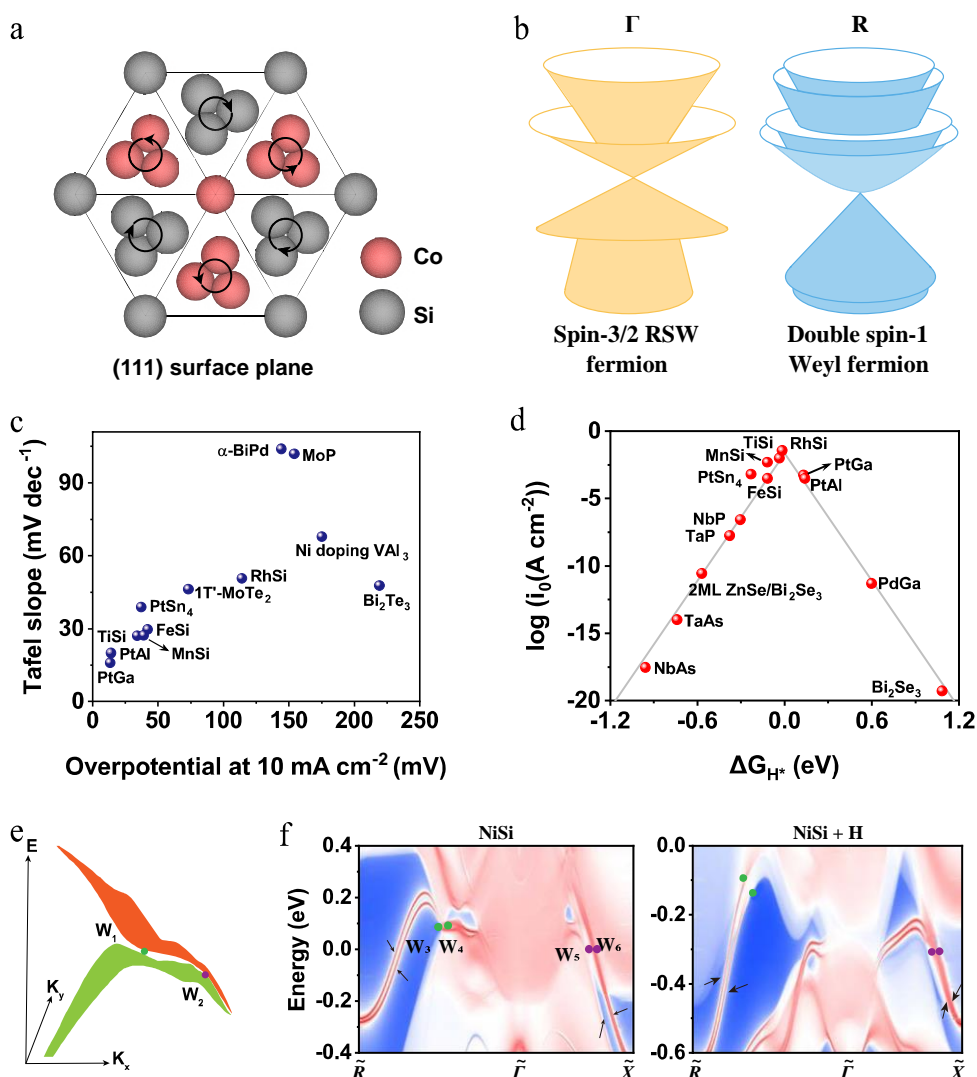


Fig. 1 | **Topological quantum materials for HER.** **a** | Schematic top view of (111) surface of topological chiral semimetal CoSi. The anticlockwise and clockwise circles indicate the chirality of the Co and Si atoms, respectively¹⁶⁷. **b** | The fourfold degenerated spin-3/2 RSW fermion node at the Γ point and the sixfold degenerated double spin-1 Weyl nodes at the R point for CoSi, coupling along the high-symmetry directions. **c** | Scatter diagram of Tafel slopes and overpotentials at 10 mA cm⁻² for metal monosilicides and other typical topological materials. Tafel slope indicates the charger transfer ability and the lower Tafel slope means the faster charge transfer ability. While the overpotential implies the extra potential for overcoming the energy

barrier to initiate the reaction. These data are collected from REFS^{9,11,13,16,38,63,64,162}. **d** | Volcano plot of various catalysts at a certain surface. These data are collected from REFS^{11,13,16,40,77}. **e** | The hybrid Weyl nodes by 3D plotting of band dispersions for NiSi. **f** | The comparison of (001) surface states of NiSi before and after the hydrogen adsorption. Panel **b** reprinted with permission from REF.⁷⁵, CC BY-NC (<http://creativecommons.org/licenses/by-nc/4.0/legalcode>). Panel **e**, **f** reprinted with permission from REF.⁸¹, Elsevier.

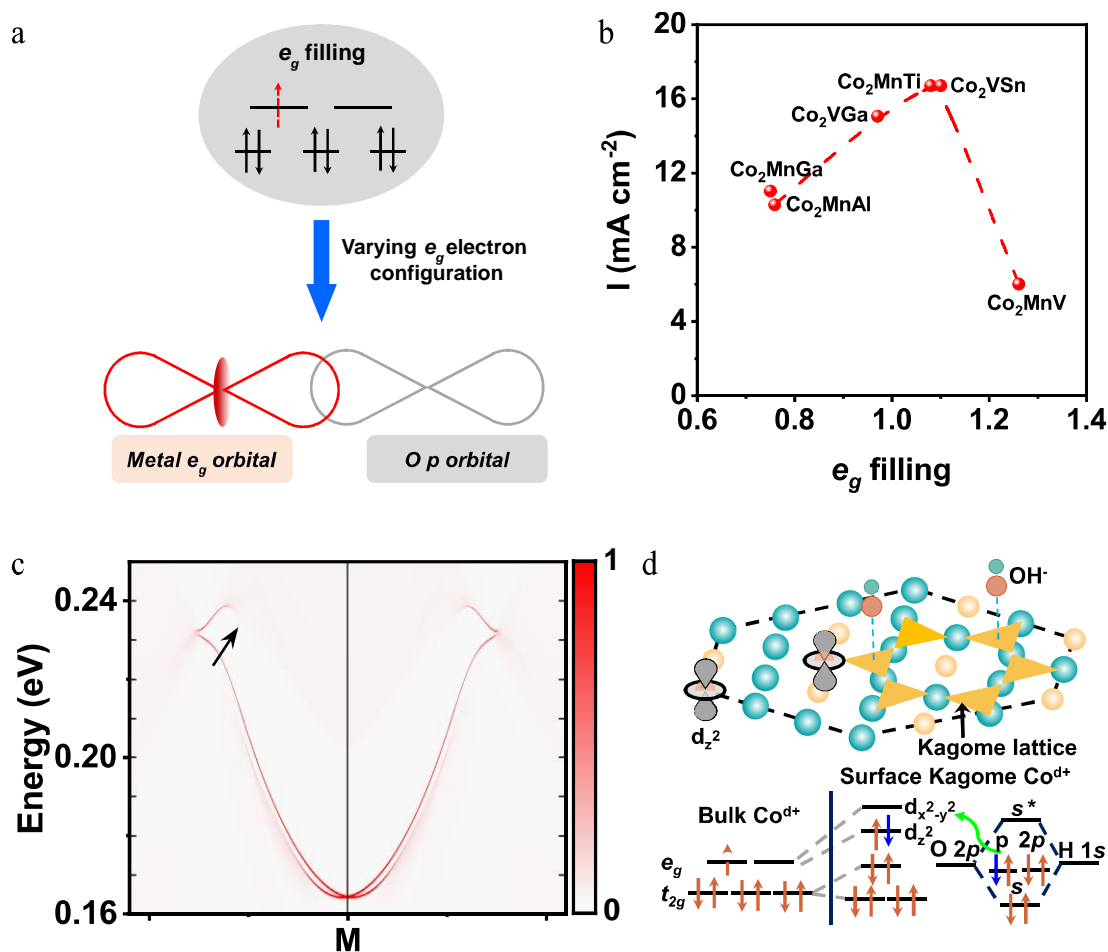


Fig. 2 | Topological materials for OER. **a** | According to the Shao-Horn (SH) principle, the binding energy of oxygen intermediates to the catalyst surface can be affected by the e_g orbital filling, and thus the OER activity can be altered by varying the e_g electron configuration. **b** | The volcano plot of the OER performance, which is derived from the current density at 1.7 V vs. RHE against the occupancy of the e_g electron of Co in Heusler compounds (Co₂MnZ and Co₂VZ). **c** | The nontrivial surface states on (001) plane of Co₃Sn₂S₂ crystal with Sn termination, which is not completely occupied and located just above the Fermi level. **d** | Schematic diagram of favourable OH uptake with the Co 3d orbitals. Panel **b** reprinted with permission from REF.⁸³, CC BY 4.0 (<https://creativecommons.org/licenses/by/4.0>). Panel **c,d** reprinted with permission from REF.¹², CC BY 4.0 (<https://creativecommons.org/licenses/by/4.0>).

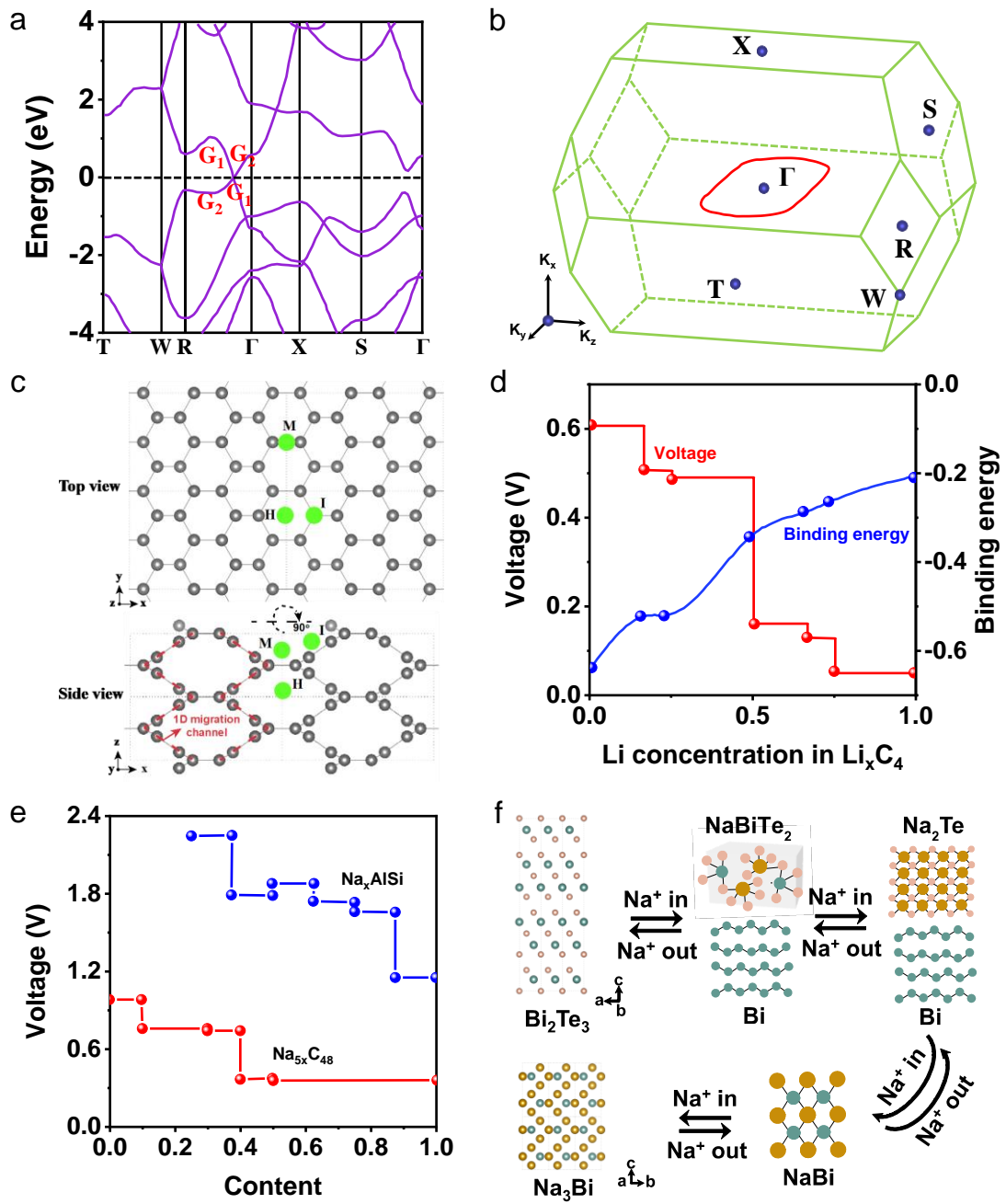


Fig. 3 | **Topological materials for battery and supercapacitors.** **a** | The bulk band structure along several high-symmetry directions for bco-C₁₆. The G1 and G2 represent the irreducible representation of the two crossing bands, respectively. **b** | The Brillouin zone of bco-C₁₆ with several high-symmetry momenta. The red circle indicates the nodal ring. **c** | Structure of bco-C₁₆ and the schematics of the possible Li-ion absorption sites in top and side view. **d** | The voltage profile and binding energy profile are calculated along the minimum energy path. **e** | The voltage profile different Na contents for four stable intermediate phases in Na_{5x}C₄₈ and the average voltage profile for

Na_xAlSi ($x = 0.25, 0.375, 0.5, 0.625, 0.75, 0.825, 1.0$) with disparate Na contents. There is a large voltage plateau (0.98 V) for $0 < x < 0.1$, which may be due to the forceful binding of Na with $t\text{C}_{24}$; the voltage is maintained around 0.75 V when $0.1 < x < 0.4$; there is an obvious decline from 0.74 to 0.37 V at $\text{Na}_{0.4t}\text{C}_{24}$ when $0.4 < x < 1.0$, as a result of the raising repulsive interaction between the Na ions. These data are collected from REFS^{90,91}. **f** | Schematic of the phase-change mechanism of Bi_2Te_3 during sodiation/desodiation process. These data are collected from REF.¹⁰⁴. Panel **a, b** reprinted with permission from REF.⁸⁹, APS. Panel **c, d** reprinted with permission from REF.⁸⁷, National Academy of Sciences.

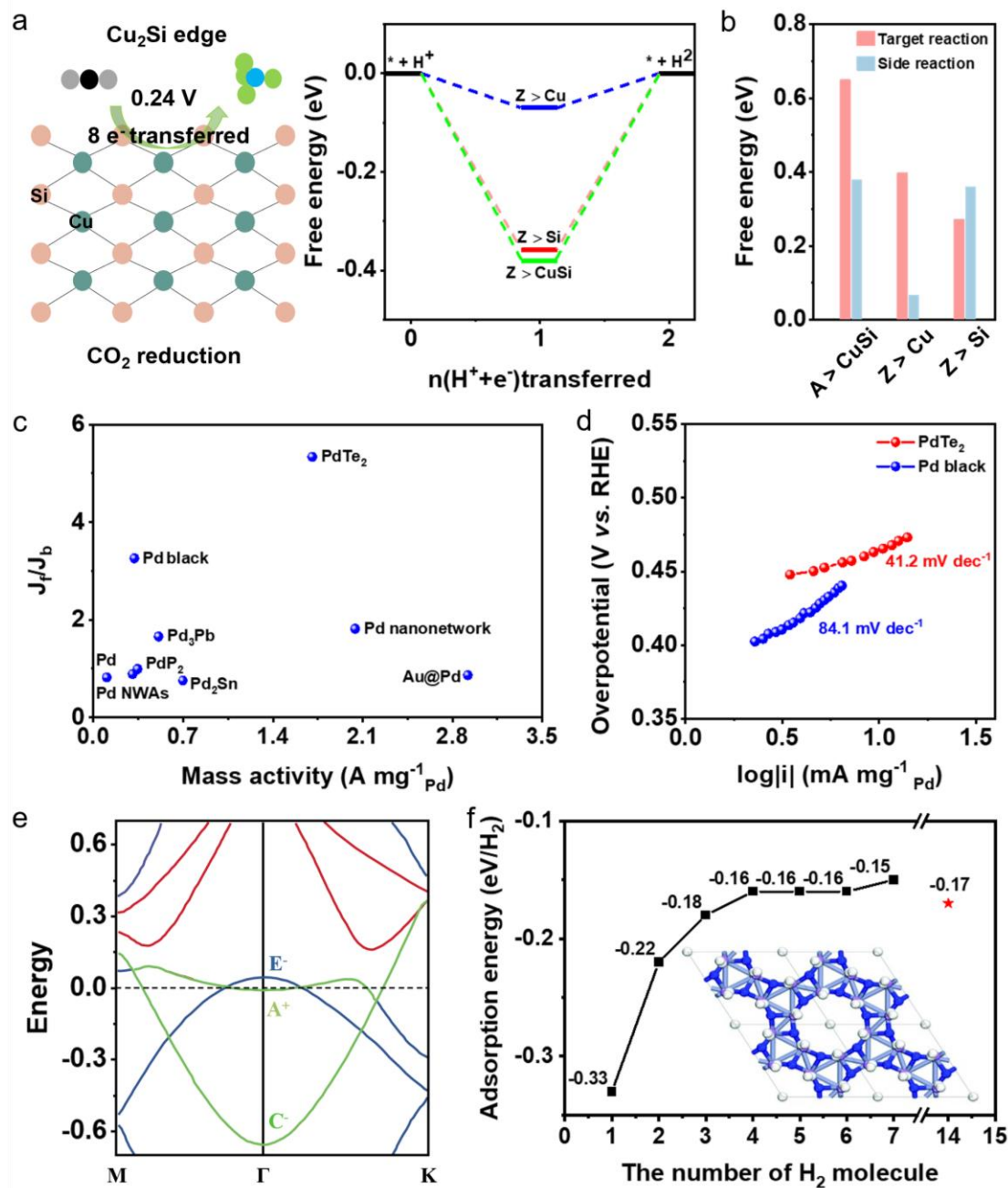
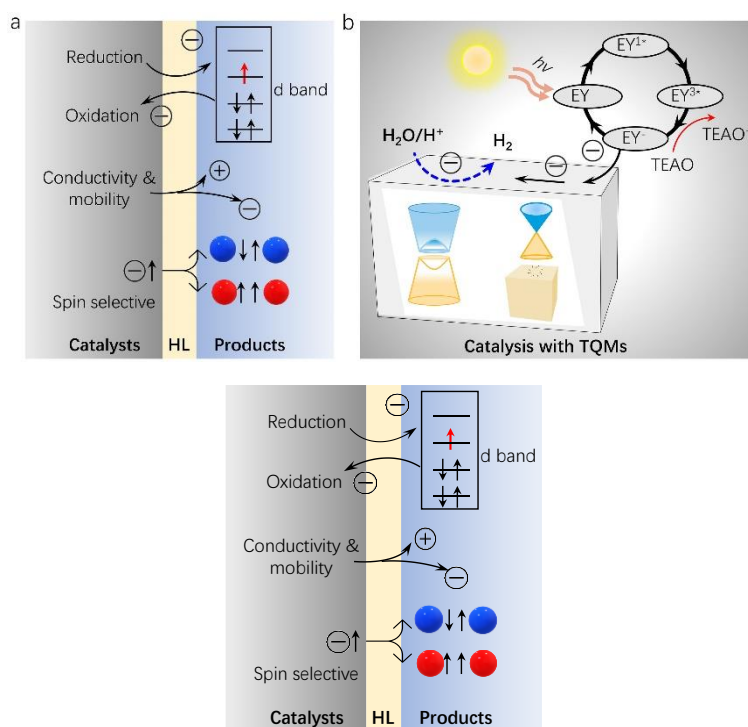


Fig. 4 | **Topological materials for other applications.** **a** | Illustration of CO_2 electro-reduction on topological nodal line semimetal Cu_2Si and side reaction profiles of nanoribbons. **b** | The comparisons of free energy change between the target reaction and the competition reaction. **c** | The comparisons of the ratio of forwarding current to backward current and mass activities between PdTe_2 nanosheets and other typical catalysts. **d** | Tafel plots of the PdTe_2 nanosheets and Pd black measures in a 1 M KOH + 1 M EtOH solution and the overpotential and current density are obtained from linear sweep voltammetry curves. **e** | The orbital-projected band structure of Li_2CrN_2 at a

strain of -10% . **f** | Changes of adsorption energies $E(\text{PBE}+\text{TS})$ with various hydrogen molecules. The optimized geometry with maximum hydrogen storage capacity is calculated according to the $G = 14 \times M(\text{H}_2)/(\text{M}(\text{Li}_2\text{CrN}_2) + 14 \times M(\text{H}_2))$, where the sign of M presents the mass. Panels **a-b** reprinted with permission from REF.¹⁴⁴, American Chemical Society. Panels **c-d** reprinted with permission from REF.¹⁰, Wiley. Panel **e** reprinted with permission from REF.¹⁴⁶, Springer Nature. Panel **f** reprinted with permission from REF.¹⁴⁷, Royal Society of Chemistry.

Box 1 General diagram for catalysis and energy conversion



Understanding chemical bonds and electron transfer are essential to describing catalysis theory from physical and chemical aspects^{168,169}. One of the most successful theories to describe catalysis is called the d -band model because d orbital electrons of the catalysts play a vital role in the process¹⁷⁰. Various linear relationships based on the d -band model have been proposed to understand the catalysis mechanisms and then predict new high-performance catalysts, such as adsorption energies of key reaction intermediates, d orbital filling numbers, and electronic spin moment¹⁷¹⁻¹⁷³. A volcano plot can be then created from the linear relationships, which

states that there is always a preferred value when the catalysis exhibits the maximum activities. For example, the Gibbs free energy of hydrogen should be neither too strong nor too weak for a good HER catalyst.

Electron transfer is an essential step for redox catalysis reactions (see panel). The essence of catalysis reactions is the electron transfer process between the catalysts and the reactants, either from the catalysts to reactants (oxidation), or vice versa (reduction). Thus, as two of the most important properties of electrons, both charge and spin should be taken into consideration. Most catalysts require high electrical conductivities to decrease the charge transfer resistances across the bulk and interface^{174,175}. High carrier mobility is another important indicator for promising catalysts. The desirable carrier mobility guarantees a fast utilization of the excited electrons for redox reactions, rather than being trapped by defects or recombination with holes^{176,177}.

In addition to conductivity and mobility, electron spin properties are often overlooked in understanding heterogeneous catalysis reactions. In fact, nearly all reaction steps, from the bond formation adsorbate, to electron transfer, can be manipulated by spin. This is because various radicals are formed during the reactions, and their reduction or oxidation is strongly dependent on the spin states of the accepted or donated electron from the catalysts. In other words, the spin states of the radical-electron pair are closely related to the electron transfer kinetics and catalytic conversion efficiencies. Such a radical-pair mechanism opens the field of spin chemistry and highlights the importance of spin electrons in high-performance designing^{178,179}.